Life Sciences 286 (2021) 120019

Contents lists available at ScienceDirect

Life Sciences

journal homepage: www.elsevier.com/locate/lifescie

# Gallocatechin-silver nanoparticle impregnated cotton gauze patches enhance wound healing in diabetic rats by suppressing oxidative stress and inflammation *via* modulating the Nrf2/HO-1 and TLR4/NF-κB pathways

Nagarjuna Reddy Vendidandala [a], Tan Pei Yin [b], Giribabu Nelli [c], Visweswara Rao Pasupuleti [a,d,e], Shaik Nyamathulla [b,*], Seri Intan Mokhtar [a,*]

[a] Faculty of Agro Based Industry, University Malaysia Kelantan, Jeli Campus, Locked bag 100, Jeli 17600, Kelantan, Malaysia
[b] Department of Pharmaceutical Technology, Faculty of Pharmacy, Universiti Malaya, 50603 Kuala Lumpur, Malaysia
[c] Department of Physiology, Faculty of Medicine, Universiti Malaya, 50603 Kuala Lumpur, Malaysia
[d] Department of Biomedical Sciences and Therapeutics, Faculty of Medicine and Health Sciences, Universiti Malaysia Sabah, Kota Kinabalu 88400, Sabah, Malaysia
[e] Department of Biochemistry, Faculty of Medicine and Health Sciences, Abdurrab University, Pekanbaru, Riau, Indonesia

ARTICLE INFO

*Keywords:*
Wound healing
Diabetes mellitus
Gallocatechin
Silver nanoparticles
Cotton gauze patches

ABSTRACT

This study is designed to investigate the combination of gallocatechin (GC) and silver nanoparticles (AgNPs) for its wound healing ability in diabetic rats. Thirty male Sprague Dawley rats were randomly divided into 5 groups: 1. Normal control rats dressed with blank CGP1; 2. Diabetic rats dressed with blank CGP1; 3. Diabetic rats dressed with 13.06μM of GC; 4. Diabetic rats dressed with 26.12 μM of GC; 5. Diabetic rats dressed with 0.1% silver sulfadiazine patches. GC-AgNPs-CGP dressed diabetic rats showed significant FBG reduction, prevented the body weight losses and reduced the oxidative stress by lowering MDA content and elevated antioxidant enzymes such as SOD, CAT and GPx in wound healing skin of diabetic rats when compared to normal CGP. Besides, mRNA expression of *Nrf2*, *Nqo-1*, and *Ho-1* was upregulated with downregulated expression of *Keap-1* mRNA, which is supported by immunohistochemistry. Furthermore, GC-AgNPs-CGP dressing increased growth factors such as VEGF, EGF, TGF-β, and FGF-2 while decreasing MMP-2 in the skin of diabetic wound rats. *In vitro* permeation study demonstrated rapid GC release and permeation with a flux of 0.061 and 0.143 mg/sq.cm/h. In conclusion, the results indicated that GC-AgNPs-CGP dressing on diabetic wound rats modulated oxidative stress and inflammation with elevated growth factors; increased collagen synthesis thereby significantly improved the wound healing and could be beneficial for the management of diabetic wounds.

## 1. Introduction

Diabetes mellitus (DM) has been a threat to human health in a large scale globally, is caused by elevated levels of glucose in blood. Day by day this metabolic syndrome is rising at an alarming pace that has affected 415 million people worldwide so far [1]. As per latest estimates of International Diabetes Federation, the annual global health expenditure on diabetes stands at USD 70 billion and is estimated that this number will reach 825 billion and 845 billion by 2030 and 2045, respectively. Among the complications that arise as a result of diabetes, delayed wound healing is one of the most debilitating complication in diabetic patients that if left untreated leads to chronic open wounds, gangrene, amputation or even death [2].

Wound healing is an intrinsic process involving dynamic changes at biochemical, molecular, immunological and physiological levels. Earlier studies revealed that delayed wound healing under diabetic mellitus is the result of elevated levels of free radicals and reduced antioxidant defences [3]. In this context, it is worth mentioning to consider the role of nuclear factor erythroid 2-related factor 2 (Nrf2) through modulation of its regulated genes in the transcriptional regulation of oxidative stress [4,5]. Furthermore, diabetic condition makes wounds stuck in a persistent inflammatory state through activation of NF-κB pathway genes and inflammatory cytokines, elevation of growth factors, lessening of matrix metalloproteinases (MMPs) and instigation of angiogenesis and epithelisation [3,6,7].

Despite having innovative technologies and synthetic drugs in place

* Corresponding authors.
*E-mail addresses:* nyamathullask@um.edu.my (S. Nyamathulla), intan@umk.edu.my (S.I. Mokhtar).

https://doi.org/10.1016/j.lfs.2021.120019
Received 2 August 2021; Received in revised form 20 September 2021; Accepted 30 September 2021
Available online 6 October 2021

to cure wound healing, none of them has accomplished the goal of successful closure without harmful effects and economic feasibility. However, medicinal plants and their bioactive compounds have attracted the public and scientific attention owing to its safety and cost effective natures. In this context, recent studies highlighted the role of catechins in the regulation of hyperglycemia, modulation of oxidative stress and inflammation and improvement in wound healing [8,9]. Gallocatechol or gallocatechin (GC), one of the main polyphenolic compounds found in green tea (*Camellia sinensis*), is a chemical compound composed of trans-isomeric gallate residue and is known for its antioxidative and inhibiting actions against lipid peroxidation [10].

Besides therapeutic efficacy, a wound healing agent should possess anti-toxic, non-allergenic properties and biocompatibility together with efficient moisture control of excess exudate. Silver is widely used for wound treatment and is approved for acute and chronic injury prevention by the Food and Drug Administration [11,12]. Silver exhibits a powerful antimicrobial activity in the form of nanoparticles [13].The silver nanoparticles (AgNPs) have shown broad-spectrum antimicrobial activity against gram-positive and gram-negative bacteria [12,14] and inhibitory action against fungal infections [15]. A study conducted by Dosoky et al. [16] and Fauda et al. [17] revealed that silver loaded silica nanoparticles are found to have antibiotic like activity upon oral administration in broiler chickens. In addition, higher cocentrations of AgNPs have demonstrated nematicidal activity and hence AgNPs were researched extensively in eco-friendly nano fertilizers [18,19]. Chitosan is a linear polysaccharide formed by partial *N*-deacetylation of chitin. Similar to silver, chitosan is a commonly used biomaterial for wound healing attributable to its heavy intermolecular hydrogen bonding, antibacterial activity and hemostasis [20]. Chitosan, gelatin and polyvinyl pyrollidone crosslinked wound dressing loaded with AgNPs downregulated β-Lactamase, mecA and erm resistance genes and enhanced the susceptibility of multidrug resistance microbes [21]. Apart from antioxidant, anti-inflammatory properties gallocatechin also possesses collagen stabilizing capabilities. The novel combination of GC-AgNPs and chitosan has the potential and was never been studied in wound healing to the best of our knowledge. Therefore, we hypothesized that this novel combination of polyphenols, silver and biodegradable chitosan would provide cost-effective system that can promote healing in a diabetic model. In view of the above, the formulation of chitosan-based gallocatechin-AgNPs impregnated cotton gauze was prepared and tested for wound healing activity in diabetic rats.

## 2. Materials and methods

### 2.1. Materials

Silver nanoparticles (AgNPs) were obtained from Chem Cruz, Heidelberg, Germany (Particle size: ≤150 nm, Purity: 99%, MW: 107.87 g/mol, Shape: Spherical). While, chitosan (low MW 50 to 190 kDa), silver sulfadiazine (98% AgS powder, molecular weight 357.14 g/mol), nicotinamide and streptozotocin (STZ) were procured from Sigma-Aldrich Company St. Louis, MO, USA. (+) - Gallocatechin (GC ≥ 98%) was obtained from ChemFaces, Wuhan, China. Strat-M® Membrane was purchased from Merck (Germany) for Franz diffusion permeation test. Whereas, other materials such as chemicals and reagents of analytical grade quality were procured and used as received.

### 2.2. Preparation of GC-AgNPs or AgS impregnated cotton gauze patches (CGPs)

Formulations of GC-AgNPs or AgS impregnated cotton gauze patches were prepared as per the composition shown in Table 1. Chitosan micronized powder (2.5 g) was accurately weighed, dissolved in 2% acetic acid (85 mL) with the aid of magnetic stirrer at 100 rpm, the mixture was heated for 30 min at 90 °C and cooled to room temperature (25 °C). Glycerine (15 mL) was added to the above solution and specified amounts of gallocatechin and AgNPs or silver sulfadiazine (AgS) in Table 1 were added into the solution. To ensure homogeneous mixing, the solution was stirred overnight and then sonicated in the bath sonicator for an hour to eliminate air bubbles (Elma, LC30H). Chitosan is cationic in nature its surface functional groups can interact with silver ions and can form composites to assist in AgNPs stabilization. Accurately measured 20 mL of the above solution was transferred on to a glass petri dish of 90 mm diameter and a similar diameter cotton gauze was soaked in the solution. The petri dish was kept in the oven for drying at 40 °C for 24 h. The GC-AgNPs or AgS impregnated dry CGP were taken out from petri dish and cut into circular patches of 28 mm diameter. To protect the matrix layer, wax papers were used on either side and individually stacked. These CGPs were kept in the silica gel desiccator prior to characterization (Table 2).

**Table 1**
Formulations of GC-AgNPs and AgS impregnated CGPs (Cotton Gauze Patches).

| Ingredients | Formulation code | | | |
|---|---|---|---|---|
| | CGP1 | CGP2 | CGP3 | CGP4 |
| Chitosan (mg) | 2500 | 2500 | 2500 | 2500 |
| AgNPs (ppm) | – | 100 | 100 | – |
| Gallocatechin (μM) | – | 13.06 | 26.12 | – |
| Silver sulfadiazine (mg) | – | – | – | 100 |
| Cotton gauze (mg) | – | q.s | q.s | q.s |
| Glycerine (mL) | 15 | 15 | 15 | 15 |
| Acetic acid (2%) up to | 100 mL | 100 mL | 100 mL | 100 mL |

### 2.3. Weight variation and thickness

The CGPs were evaluated for weight variation and uniformity in thickness. Five patches were randomly selected from each formulation, weighed on electronic digital balance to check accuracy of weight and ensure less than 5% variation. To analyse the uniformity of thickness, measurements for individual CGPs were made at the centre and four corners using Vernier Callipers of 0.01 mm accuracy. The tests were repeated for five times to minimize variation (Table 2).

### 2.4. Tensile strength

The breaking point of CGP was determined using a Brookfield's CT-3 texture analyzer with an initial grip spacing of 10 mm and a steady speed of 1 mm/s (Table 2). Tensile strength (kg/cm$^2$) was determined by dividing maximum load and cross-sectional area. Elongation at break (%) was calculated using the following equation.

**Table 2**
Physicochemical properties of prepared CGP1 to CGP4 (Mean ± SD; $n = 5$).

| Test | Formulation code | | | |
|---|---|---|---|---|
| | CGP1 | CGP2 | CGP3 | CGP4 |
| Weight variation (mg) | 469.40 ± 29.08 | 430.70 ± 10.62 | 413.90 ± 11.63 | 462.18 ± 14.14 |
| Thickness (mm) | 0.38 ± 0.05 | 0.55 ± 0.03 | 0.56 ± 0.02 | 0.58 ± 0.04 |
| Tensile strength (kg/cm$^2$) | 0.02 ± 0.01 | 0.44 ± 0.03 | 0.43 ± 0.05 | 0.43 ± 0.05 |
| Elongation at break (%) | 28.16 ± 2.86 | 47.20 ± 2.23 | 46.66 ± 3.48 | 46.06 ± 1.54 |
| Folding endurance (times) | 27 ± 5.34 | >300 | >300 | >300 |
| Moisture content (%) | 9.16 ± 0.62 | 6.58 ± 0.55 | 7.10 ± 0.27 | 10.70 ± 0.21 |
| Water absorption test (%) | 197.06 ± 13.47 | 90.00 ± 3.99 | 87.75 ± 4.68 | 84.10 ± 4.68 |
| Gallocatechin/AgS content (%) | – | 93.47 ± 5.85 | 93.22 ± 8.72 | 91.47 ± 5.52 |

$$\text{Elongation at break } (\%) = \frac{\text{CGP elongation at break}}{\text{Initial CGP length}} \times 100$$

### 2.5. Folding endurance

The CGPs were analysed for the resilience towards wear and tear. Each CGP was consistently folded in the same place until it was either split or cracked to a limit of 300 times [22]. The number of times the patches fold in the same position without breakage is determined, the folding durability values are shown in Table 2.

### 2.6. Moisture content

The estimation of moisture levels can help to assess the conducive environment for microbial growth and hydrolysis. CGPs were initially weighed and placed in a desiccator containing silica gel dehydrating agent. The CGPs were weighed repeatedly until they showed constant weights. The moisture content (%) was calculated by the following equation [22].

$$\text{Moisture content } (\%) = \frac{\text{Initial weight} - \text{Dry weight}}{\text{Initial weight}} \times 100$$

### 2.7. Water absorption test

The CGP samples were immersed in 40 mL of distilled water at room temperature for 5 min to know the water absorption capacity of the dry patches. They were taken out from the beaker, air-dried at room temperature for two minutes and reweighed [23] to calculate percent water absorption by using the following formula.

$$\text{Water absorption } (\%) = \frac{\text{Final weight} - \text{Initial weight}}{\text{Initial weight}} \times 100$$

### 2.8. Vertical wicking test

A 60 mm long and 10 mm wide strips of CGPs were vertically sliced and hanged vertically in a beaker filled with distilled water and ensured that only one end of the strip was submerged to a depth of 10 mm in water. Wicked water heights were recorded after 10 min [23].

$$\text{Flux } (\text{mg/sq.cm/h}) = \frac{\text{Amount permeated}}{\text{Cross sectional area of CGP exposed to PBS}} \times \text{Time for diffusion}$$

### 2.9. Estimation of gallocatechin content

The CGPs were cut into $1 \times 1$ cm$^2$ size pieces and then GC or AgS was extracted by dissolving in 10 mL of phosphate buffer solution (pH 7.4) subjecting it for constant stirring. GC or AgS free patches were handled equally to serve as blank. The amount of GC or AgS present in the buffer was determined by analysing at 210 and 254 nm respectively by UV–Visible spectrophotometer (Shimadzu UV-1601) (Table 1).

### 2.10. Fourier Transform Infrared Spectroscopy (FTIR) study

FTIR spectrophotometer was used to characterize pure samples, mixtures and to study the drug interactions between the components that might have involved functional groups. The KBr pellet for samples was prepared by pelletization method containing 1 part of sample to 100 parts of KBr and compressed pellet was scanned over a wavenumber range of 4000–400 cm $^{-1}$ to record bending, stretching vibrations or deformation bands of the molecules. The FTIR spectra obtained were as shown in Fig. 2A.

### 2.11. Differential Scanning Calorimetry (DSC) study

Differential scanning calorimetry was used to check any possible interactions among the excipients and GC, to know the phase transitions of the samples in order to characterize the physical state by using NETZSCH DSC 200 F3 (Germany). Samples of known mass were placed in aluminium pans and hermetically sealed. The samples were heated from 30 to 300 °C at a heating rate of 10 °C/min in an inert nitrogen atmosphere to prevent oxidation, nitrogen as the purge gas. The DSC instrument was calibrated for temperature using Indium. DSC thermograms of the samples and excipient combinations of the formulations was analysed by the thermal analyzer. The interaction of the components, melting points and purity of the samples were analysed and the thermograms were recorded as shown in Fig. 2B.

### 2.12. Drug permeation study

The study was conducted in a three station Franz diffusion cell apparatus, the individual Franz cell was filled with PBS (pH 7.4) with a receptor volume of $5 \pm 0.1$ mL and it had a surface area of 0.64 cm$^2$. In this test, Strat-M® membrane was used replacing animal skin model. Each test sample (CGP) was mounted on to the Strat-M® membrane and clipped between the donor and the receptor orifice. The temperature of the receptor compartment was held at $37 \pm 0.5$ °C in a circulated water bath. The sample ports were covered with parafilm to avoid evaporation and contamination. The magnetic stirrer with a speed of 50 rpm was used for continuous stirring of the receiver medium to ensure uniform distribution of PBS and maintain the sink condition. Aliquots of 0.5 mL were removed from the receptor compartment using a syringe at various time points *i.e.*, 0.25, 0.5, 1, 2 and 4 h. Each 0.5 mL sample was diluted with PBS (pH 7.4) and absorbance was measured at 210 nm or 254 nm using UV–Visible spectrophotometer (Shimadzu, UV-1601). The Flux and percent release were calculated from the *in vitro* permeation analysis using the following equations.

$$\text{Percent release } (\%) = \frac{\text{Amount permeated}}{\text{Amount present in CGP}} \times 100$$

### 2.13. Animal experiments

Six to eight weeks Sprague Dawley (SD) male rats were obtained from Universiti Malaya, Kuala Lumpur, Malaysia and housed in polypropylene cages at a temperature and humidity regulated atmosphere ($23 \pm 1$ °C; 40–60%) by providing 12 h dark or light at cycles. The rats in the experiment had free access to water (Reverse osmosis and autoclaved) and food *ad libitum* and standard animal feed. Before the study ethical committee approval (2019-210806/PHYSIO/R/GN) was received from institutional animal ethics committee, Faculty of Medicine, Universiti Malaya, Kuala Lumpur, Malaysia.

### 2.14. Induction of diabetes

Diabetes was induced in rats by injecting single intraperitoneal

injections of nicotinamide (110 mg/kg body weight) in saline and streptozotocin (STZ) (55 mg/kg body weight after 15 min of nicotinamide injection) in 0.1 mol/L citrate buffer (pH 4.5). The diabetes was confirmed after 72 h of STZ injection by evaluating fasting blood glucose levels through Accu-Chek glucose meter (Roche Diagnostics, Basel, Switzerland). Animals showing glucose levels above 12.5 mmol/L were considered diabetic and selected for the experiment.

### 2.15. Wound creation in diabetic rats

Rats were anaesthetized by intraperitoneal injection of ketamine (50 mg/kg) and xylazine (5 mg/kg), their back skin was shaved and single full-thickness excisional wounds of 2 cm were created with sterile punch (Stiefel laboratories, Carolina, USA). Surgical region was surface sterilized with chlorhexidine, 70% ethanol and iodine. After recovering from anaesthesia, animals were individually housed in cages. Wound created animals were randomly divided into 5 groups with 6in each group.

Group I: Non-diabetic (normal control) rats dressed with blank cotton gauze patches (NC-CGP1)
Group II: Diabetic (diabetic control) rats dressed with blank cotton gauze patches (DC-CGP1)
Group III: Diabetic rats dressed with 13.06 μM GC-AgNPs cotton gauze patches (CGP2)
Group IV: Diabetic rats dressed with 26.12 μM GC-AgNPs cotton gauze patches (CGP3)
Group V: Diabetic rats dressed with silver sulfadiazine (AgS) cotton gauze patches (CGP4)

In the experimental animals wound contraction and healing periods were calculated on 0, 3, 6, 9, 12, 15 and 18 days. Wound region was regularly tracked with a planimetric calculation and images of the same were taken at the above-mentioned time points and then measured by Image J software (1.47v, NIH, Bethesda, USA) to determine the uncured wound scale. Wound region was dressed with CGPs from 0 to 18 days.

The percentage of wound closure was calculated as:

$$= \frac{\text{area of actual wound}}{\text{area of original wound}} \times 100$$

Normal control rats were euthanized on day 16 and remaining groups on day 19 after the surgery and a full-thickness cutaneous wound healing and neighbouring tissues were collected. The excised skins were immersed in 10% formalin at room temperature. During processing of tissues for histopathology examination, initially tissues were dehydrated in ascending alcohol series (70, 80, 90, 95, and 100%), placed in paraffin blocks and sliced into 5 μm thick sections. Sections were stained with hematoxylin/eosin and Masson's trichrome stains for microscopic examination.

### 2.16. Immunohistochemistry staining

For immunohistochemistry staining, tissue sections were initially dewaxed in xylene and rehydrated in descending alcohol series. The sections were submitted for antigen retrieval process and blocked endogenous peroxidase activity by keeping it in 3% $H_2O_2$ at room temperature for 30 min. Then unwanted binding was blocked with blocking one solution (Nacalai Tesque, Kyoto, Japan) at 37 °C for 30 min and later incubated with primary antibodies to Nrf2 (NBP1-32822), HO-1 (NBP1-97507), MYD88 (NB100-56698), TNF-α (NBP1-19532), VEGF (sc-507), FGF2 (sc-1360) and MMP2 (sc-8835) (Novus Biologicals and Santa Cruz, CA, USA) at 4 °C overnight, followed by the secondary antibody incubation at 37 °C for 1 h. Slides were then incubated in avidin-biotin complex (Boster) at 37 °C for 20 min and diaminobenzidine (DAB) for 5 min. Finally, the positive areas were observed under inverted microscope (BX-51, Olympus, Japan).

### 2.17. Immunofluorescence staining

For immunofluorescence analyses, sections were deparaffinized in xylene, dehydrated in alcohol, submitted for antigen retrieval process and blocked with block ONE incubation at room temperature for 30 min. After overnight incubation at 4 °C with primary antibodies (anti-NF-kB p65 (sc-8008, Santa Cruz, CA, USA), anti-EGF (sc-374255, Santa Cruz, CA, USA) and TGFβ (sc-146, Santa Cruz, CA, USA) at 1:1000 ratio, the slides were incubated with FITC/PE secondary antibodies (1:200) at room temperature for 1 h and counterstained with DAPI and examined under confocal microscopy.

### 2.18. Determination of oxidative and anti-oxidative status

Levels of MDA [24] as a measure of oxidative stress and enzyme activities of SOD [25], CAT [26] and GPx [27] as a measure of anti-oxidative defence system were determined in the wound tissue homogenate using standard protocols. The levels of MDA and enzyme activities of SOD, CAT and GPx were measured as mmol/mg protein and U/mg protein, respectively.

### 2.19. Real time PCR study

Total mRNA from the wound tissues of control and experimental rats was extracted with the help of Trizol reagent method (Invitrogen, Carlsbad, CA). RNA (1 μg) was then further processed to synthesize cDNA by reverse transcription method by Thermo Scientific kit (Burlington, Canada). The cDNA samples were then processed using RT-PCR reaction (10 ng of cDNA, 9 μL of qPCR Master Mix and 20 μL of respective primers) using SYBR® Premix Ex Taq™ (Tli RNaseH Plus) (Applied Biosystems, Foster City, CA). The resultant qPCR data was analyzed by DDCT method. The relative expression of target genes was quantified with the help of Ct values and $2^{-\Delta\Delta CT}$ method. β-actin was used as a house keeping gene.

### 2.20. Statistical analysis

The data were expressed as mean ± standard deviation (SD) of at least three independent experiments. Differences were performed by One-way ANOVA using the SPSS 17.0 (SPSS Inc., Chicago, IL, USA) software. A value of $p < 0.05$ was considered as statistically significant.

## 3. Results

Physicochemical properties of CGPs were determined to ensure that the prepared patches have the characteristics of desired transdermal drug delivery system. Formulation CGP1 was prepared with no cotton gauze, thus it was clear and appeared as transparent film. Presence of gallocatechin in the formulation gave yellowish tinge. However, CGP3 had a darker yellowish colour compared to CGP2 as it contained higher concentration of gallocatechin as shown in Table 1. However, CGP4 were slightly greyish due to the presence of silver sulfadiazine, which is devoid of GC [28]. Prepared CGPs were evaluated for weight variation, thickness, tensile strength, folding endurance, moisture content, water absorption test, vertical wicking test, FTIR, DSC, gallocatechin content and GC/AgS permeation study.

### 3.1. Weight variation and thickness

Weight variation is conducted to examine the intra-batch variability of patches. The results of each formulation are shown in Table 2. CGP1 has the largest mean value of 469.40 ± 29.08 mg and the CGP3 had the least mean value of 413.90 ± 11.63 mg. CGP2 and CGP4 had the weight variation of 430.70 ± 10.62 and 462.18 ± 14.14 respectively. The thickness of the patches ranged between 0.38 ± 0.05 and 0.58 ± 0.04 mm.

### 3.2. Tensile strength and elongation at break

Wound dressing should be durable, stress resistant and flexible in order to handle the stresses exerted by different body parts [29]. These characteristics can be examined through tensile strength and elongation at break that correlate with the strength and elasticity of the patches, respectively. The results of tensile strength and elongation at break of different CGPs were presented in Table 2. Blank film without cotton gauze (CGP1) had lowest tensile strength and elongation at break of $0.02 \pm 0.01$ kg/cm$^2$ and $28.16 \pm 2.86$% respectively. Presence of cotton gauze has improved the stiffness and elasticity of the patches, CGP2 showed high tensile strength of $0.44 \pm 0.03$ and large percent elongation at break of $47.20 \pm 2.23$ as shown in Table 2. Percent elongation at break measures the flexibility of a wound dressing and it is considered as an important parameter during application or removal from the wound site [30]. Tensile properties of the patch can also be explained with the stress-strain curve as shown in Fig. 1J and K. It is noticed that CGP1 broke into 2 parts once the tensile strength is applied while the gauze patch remained elongated (Fig. 1).

### 3.3. Folding endurance

Folding endurance measures the ability of patches to withstand the external force and it is correlated with the mechanical properties. High folding endurance number indicates high mechanical properties for CGPs indicating their integrity during general skin folding [31]. As shown in Table 2, CGP1 showed the lowest folding endurance (27 times) and developed a furrow while the rest of the formulations (CGP2 to CGP4) were found to withstand folding more than 300 times primarily due to the network of cotton and other components. Addition of gauze backing layer has significantly increased the folding endurance of the patches and improved their flexibility. Flexibility is prerequisite for wound dressing as it will directly influence the conformability of the dressing. All patches with gauze impregnated layer (CGP2 to CGP4) showed good flexibility.

### 3.4. Moisture content

Moisture content measurement is one of the crucial factors that affect fluid or exudate uptake in a wound by the patches [32]. It can also affect the drug release from the matrix layer and microbial growth in CGPs. The CGPs demonstrated moisture levels between $6.58 \pm 0.55$ to $10.70 \pm 0.21$ and interestingly the gallocatechin bearing CGPs (CGP 2: $6.58 \pm 0.55$; CGP3: $7.10 \pm 0.27$) showed low moisture content. Low percent of moisture content may provide greater stability, longer shelf life and prevent formation of dried and brittle dressing [22].

### 3.5. Water absorption test

Water absorption percentages of CGPs are shown in Table 2. The CGP1 had the highest percentage ($197.06 \pm 13.47$) of water absorption and the lowest was observed in CGP4 with $84.10 \pm 4.68$%. Addition of cotton gauze is expected to increase water absorbability of the patches. However, the results did not support the assumption due to the formation of water insoluble chitosan matrix around the cotton fibre hindering its water absorbability. Perhaps due to chitosan being an acid-soluble and water-insoluble polymer it might have reduced the water absorption capacity.

### 3.6. Vertical wicking test

The CGP1 showed a good water absorbability and transferability. Addition of gallocatechin into the formulation (CGP2 and CGP3) improved the water absorption rate compared to silver sulfadiazine (CGP4) slightly. However, CGP1 exhibited significantly higher capillary action compared to its counterparts. The CGP1 had 4.4 mm height of wicked water in comparison to 2.8, 2.8 and 2.2 for CGP2, CGP3 and CGP4 respectively. Good water absorption rate is an indication that CGPs can absorb exudates, attach to the wound for a longer time and may improve the rate of drug release at the wound site.

### 3.7. Estimation of gallocatechin content

As described previously by Vinklárková et al. *[33]*, the preparation of transdermal patches should contain 90 to 110% of stated drug content. The GC/AgS contents of CGP2, CGP3 and CGP4 were examined as per the method described earlier. The calculated amounts of GC/AgS in CGP2, CGP3 and CGP4 were $93.47 \pm 5.85$, $93.22 \pm 8.72$ and $91.47 \pm 5.52$% respectively. The result showed that the method employed for

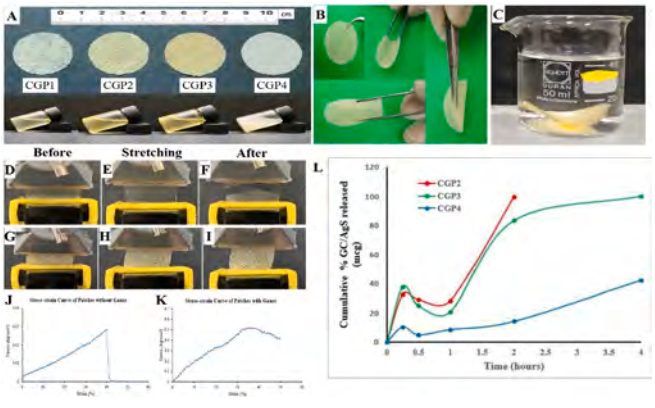


**Fig. 1.** GC-AgNPs or AgS impregnated cotton gauze patches and their physicochemical characterization A) Prepared CGP1 to CGP4 circular patches of 28 mm diameter which are investigated for wound healing along with respective liquid suspension used for impregnation of cotton gauzes; B) A representative patch of CGP3 with its three-dimensional view and flexibility; C) Image showing CGP in a beaker during water absorption test; D) CGP1 before tensile strength test; E) CGP1 stretched; F) CGP1 at the end of the test; G) CGP3 before tensile strength test; H) CGP3 stretched; I) CGP3 at the end of the test; J) Stress-strain curve of CGP1; K) Stress-strain curve of CGP3; L) Permeation profiles of CGP2, CGP3 and CGP4 across Strat-M® membrane.

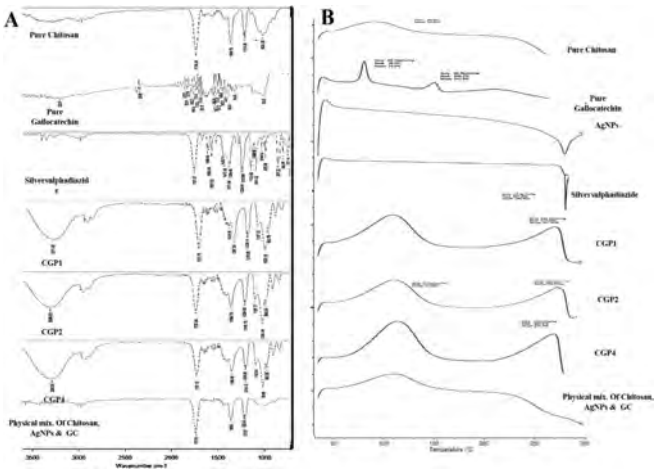


**Fig. 2.** Assessment of compatibility of GC and AgS with other formulation components evaluated by FTIR and DSC during preformulation study. A) FTIR spectra of pure chitosan, gallocatechin, AgS and when in CGP1, CGP2, CGP4 showing bands of stretching, bending and deformations, the spectra of a simple physical mixture of CGP2 raw materials to evaluate the physical interaction; B) DSC thermograms of pure chitosan, gallocatechin, AgS and when in CGP1, CGP2, CGP4 showing broad and sharp peaks indicating crystallinity, phase transition, impurity and interactions, a simple physical mixture of CGP2 raw materials to evaluate the physical interaction.

preparing CGP is capable of giving uniform GC/AgS content with minimum batch variability and good homogeneity.

### 3.8. Fourier Transform Infrared Spectroscopy (FTIR) study

In Fig. 2A FTIR spectra of pure GC showed functional peaks at 3203.57 $cm^{-1}$ (O—H stretching), 1691.79 $cm^{-1}$ (C═C stretching) and 1345.56 $cm^{-1}$ (Phenol C—O stretching) representing structural features of the molecule. Pure chitosan demonstrated functional peaks at 1738.24 $cm^{-1}$ (N—H bending), 1366.79 $cm^{-1}$ (C—H stretching), 1216.28 $cm^{-1}$ (Phenol C—O band) and 1024.35 $cm^{-1}$ (N—C stretching). Similarly, pure AgS had important peaks at 1737.27 $cm^{-1}$ (N—H bending), 1596. 64 $cm^{-1}$ (C═C stretching) and 1229.64 $cm^{-1}$ (C—O stretching). CGPs did not demonstrate any major changes in peak positions, shifting of peaks and broadening of the peaks, no obvious functional group changes in the FTIR spectra of individual components were noticed indicating retention of functional groups even after formulation.

### 3.9. Differential Scanning Calorimety (DSC) study

The Fig. 2B represents the thermograms of pure chitosan, gallocatechin, AgS, AgNPs as well as CGPs. The pure chitosan showed a broad endothermic peak at 90.6 °C, gallocatechin had two sharp endothermic peaks at 78.2 °C and 148.2 °C. AgS exhibited a sharp exothermic peak at 297.1 °C, the physical mixture of raw materials predominantly showed similar thermogram like that of pure chitosan due to its large weight ratio. The CGPs demonstrated broad endothermic peaks between the 104.9–121.5 °C and 268.4–285.8 °C suggesting broadening and shifting of peaks indicating physical interactions between raw materials leading to loss of crystalline behaviour of pure compounds.

### 3.10. GC/AgS permeation study

Franz diffusion cell was used to study *in vitro* GC/AgS permeation. Fig. 1L depicts the permeation profiles of CGP2, CGP3 and CGP4 in PBS (pH 7.4) at 37 ± 0.5 °C against time. Initial burst release was noticed from the CGPs within 15 min in all the three formulations. There was 32.64, 37.76 and 10.42% GC/AgS release from CGP2, CGP3, CGP4 respectively at 15 min time point. After that there was a short lag phase between 0.5 and 1 hour in all the CGPs and a fall in percentage was observed. At 30 min 29.18, 24.93 and 4.90% was recorded respectively from the same CGPs. It was further dropped at 1 h to 28.32 and 20.62% in CGP2, CGP3 respectively, contrary to this CGP4 reversed the fall and showed 8.48 % from its earlier time point. The GC/AgS was released gradually from the patches after one hour. Gallocatechin was 99.64% released from the chitosan matrix within 2 h in CGP2 in comparison to 83.21% from CGP3 as shown in Fig. 1L. However, CGP3 released 100% at 4 h whereas formulation CGP4 released 49.09 % of AgS. Permeation rate or flux of gallocatechin in CGP3 was 0.143 compared to 0.061 mg/sq.cm/h of CGP2. The flux of AgS in CGP4 was found to be 0.378 mg/sq.cm/h due to its high initial drug load.

### 3.11. Effect of GC-AgNPs-CGPs on body weight and blood glucose levels in diabetic rats

Fig. 3A illustrates the effect of GC-AgNPs-CGP on mean weekly bodyweight. On Day 0, there was no significant difference in body weight among all groups ($p > 0.05$), but diabetic rats dressed with blank cotton gauze patches (DC-CGP1) showed significant ($p < 0.05$) decrease in body weight on days 6, 12 and 18 as compared to normal control rats dressed with blank cotton gauze patches (NC-CGP1). Besides, diabetic rats dressed with 13.06 μM GC-AgNPs and 26.12 μM GC-AgNPs-CGPs (CGP2 and CGP3) prevented body weight loss as compared to diabetic rats dressed with blank cotton gauze patches (DC-CGP1).

The effect of GC-AgNPs-CGP on blood sugar levels was depicted in

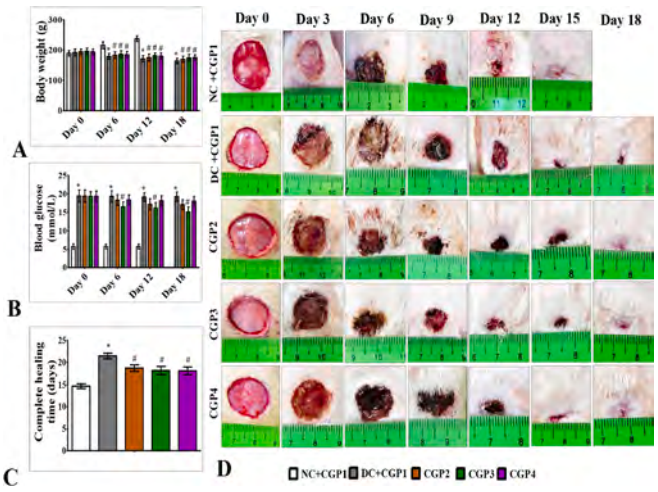


**Fig. 3.** Effect of GC-AgNP CGPs dressing on metabolic parameters and wound healing time in diabetic rats. (**A**) Body weight; (**B**) Blood glucose; (**C**) Complete wound healing time; **(D)** Wound healing pictures on different days; NC + CGP1: Normal control dressed with blank cotton gauze; DC + CGP1: Diabetic control rats dressed with blank cotton gauze; CGP2: Diabetic rats dressed with 13.06 μM gallocatechin and silver nanoparticle (GC-AgNP) impregnated cotton gauze patches (DC+ 13.06 μM CGP2); CGP3: Diabetic rats dressed with 26.12 μM gallocatechin and silver nanoparticle (GC-AgNP) impregnated cotton gauze patches (DC+ 26.12 μM CGP3). CGP4: Diabetic rats dressed with silver sulfadiazine (DC + AgS) impregnated cotton gauze patches. Data were expressed as mean ± S.E.M ($n = 6$). *$p < 0.05$ compared to control, # $p < 0.05$ compared to DC.

Fig. 3B. Diabetic rats dressed with DC-CGP1 had significantly higher blood glucose levels when compared to normal control rats dressed with NC-CGP1. Diabetic rats dressed with 26.12 μM GC-AgNPs (CGP3) had significantly ($p < 0.05$) lower blood glucose levels on days 6, 12 and 18 when compared to DC-CGP1.

### 3.12. Effect of GC-AgNPs-CGPs on wound healing in diabetic rats

Fig. 3D displays the images of wound healing belonging to each category of rats on days 0, 3, 6, 9, 12, 15, and 18 following wound creation. Fig. 3C indicates the total duration of wound healing (days) on experimental rats. DC-CGP1 dressed rats had a significantly longer wound healing period than NC-CGP1 dressed rats. In comparison to diabetic rats, 13.06 μM CGP2 and 26.12 μM CGP3 had significantly ($p < 0.05$) lower wound healing time.

### 3.13. Effect of GC-AgNPs-CGPs on histopathology in diabetic rats

Histological examination of skin of various experimental groups was seen in Fig. 4A. The skin sections of the NC-CGP1 dressed rats displayed normal skin histological features with clear keratin sheet, intact basement membrane, epidermis and dermis with associated structures (hair follicles, sweat and sebaceous glands). In contrast, the wounded area of skin in the diabetic rats exhibited serious histologic alterations in the form of complete loss of epithelial cover exposing the underlying tissue and wound gap filled with irregularly arranged granulation tissue with inflammatory cell infiltrations. Additionally, neovascularisation was observed at the base of wound. While, significant improvement was observed in 13.06 μM CGP2 and 26.12 μM CGP3 dressed diabetic rats in the form of optimal re-epithelisation, epidermal remodelling, dermal reconstruction and the surface was fully covered by a thick sero-cellular crust composed of necrotic tissue debris and inflammatory exudates. Furthermore, decreased collagen was observed in skin histological sections of diabetic rats but increased collagen was observed in Masson's trichrome stained sections of diabetic rats dressed with 13.06 μM CGP2

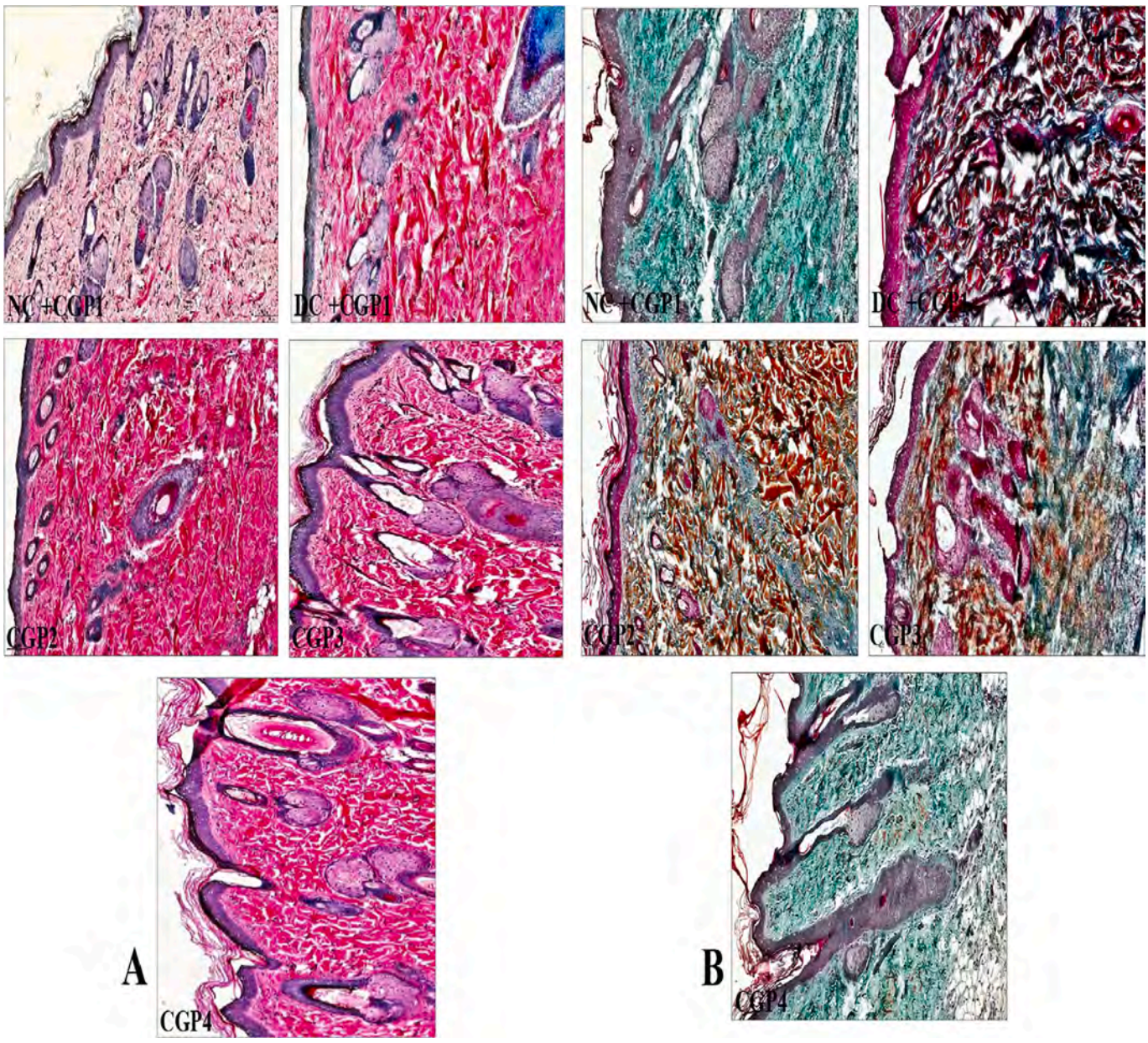


**Fig. 4.** Effect of GC-AgNP CGPs dressing on histopathology in diabetic rats. **(A)** H & E; **(B)** Masson trichrome staining. NC + CGP1: Normal control dressed with blank cotton gauze; DC + CGP1: Diabetic control rats dressed with blank cotton gauze; CGP2: Diabetic rats dressed with 13.06 μM gallocatechin and silver nanoparticle (GC-AgNP) impregnated cotton gauze patches (DC+ 13.06 μM CGP2); CGP3: Diabetic rats dressed with 26.12 μM gallocatechin and silver nanoparticle (GC-AgNP) impregnated cotton gauze patches (DC+ 26.12 μM CGP3). CGP4: Diabetic rats dressed with silver sulfadiazine (DC + AgS) impregnated cotton gauze patches. Scale bar = 100 μm.

and 26.12 μM CGP3 (Fig. 4B).

### 3.14. Effect of GC-AgNP-CGPs on oxidative and anti-oxidative parameters in diabetic rats

DC-CGP1 dressed rat healing tissues exhibited lower mRNA expression of *Nrf2* (Fig. 5A), *Nqo1* (Fig. 5C) and *Ho-1* (Fig. 5D) and higher *Keap-1* mRNA expression (Fig. 5B) when compared to NC-CGP1 dressed rats. However, there was a significant increase in *Nrf2*, *Nqo1* and *Ho-1* with decreased *Keap-1* mRNA expression in topically applied 13.06 μM CGP2 and 26.12 μM CGP3 dressed diabetic rats compared to diabetic rats. Malondialdehyde (MDA), lipid peroxidation (LPO) product content in healing tissue was significantly higher in DC-CGP1 dressed rats compared to NC-CGP1 dressed rats (Fig. 5E). In addition, antioxidant enzymes such as SOD (Fig. 5F), CAT (Fig. 5G) and GPx (Fig. 5H) levels were significantly ($p < 0.05$) decreased in healing tissues of DC-CGP1 dressed rats when compared with healing tissues of NC-CGP1 dressed rats. However, these antioxidant enzyme levels were significantly increased and MDA levels were significantly decreased in diabetic rats dressed with 13.06 μM CGP2 and 26.12 μM CGP3 compared to DC-CGP1 dressed rats.Immunohistochemistry results showed that DC-CGP1 dressed healing tissues showed lower distribution of Nrf2 (Fig. 6A) and HO-1 (Fig. 6B) as compared to NC-CGP1 dressed rats. Whereas diabetic rats dressed with 13.06 μM CGP2 and 26.12 μM CGP3 showed higher distribution of Nrf2 and HO-1 when compared to DC-CGP1 dressed rats.

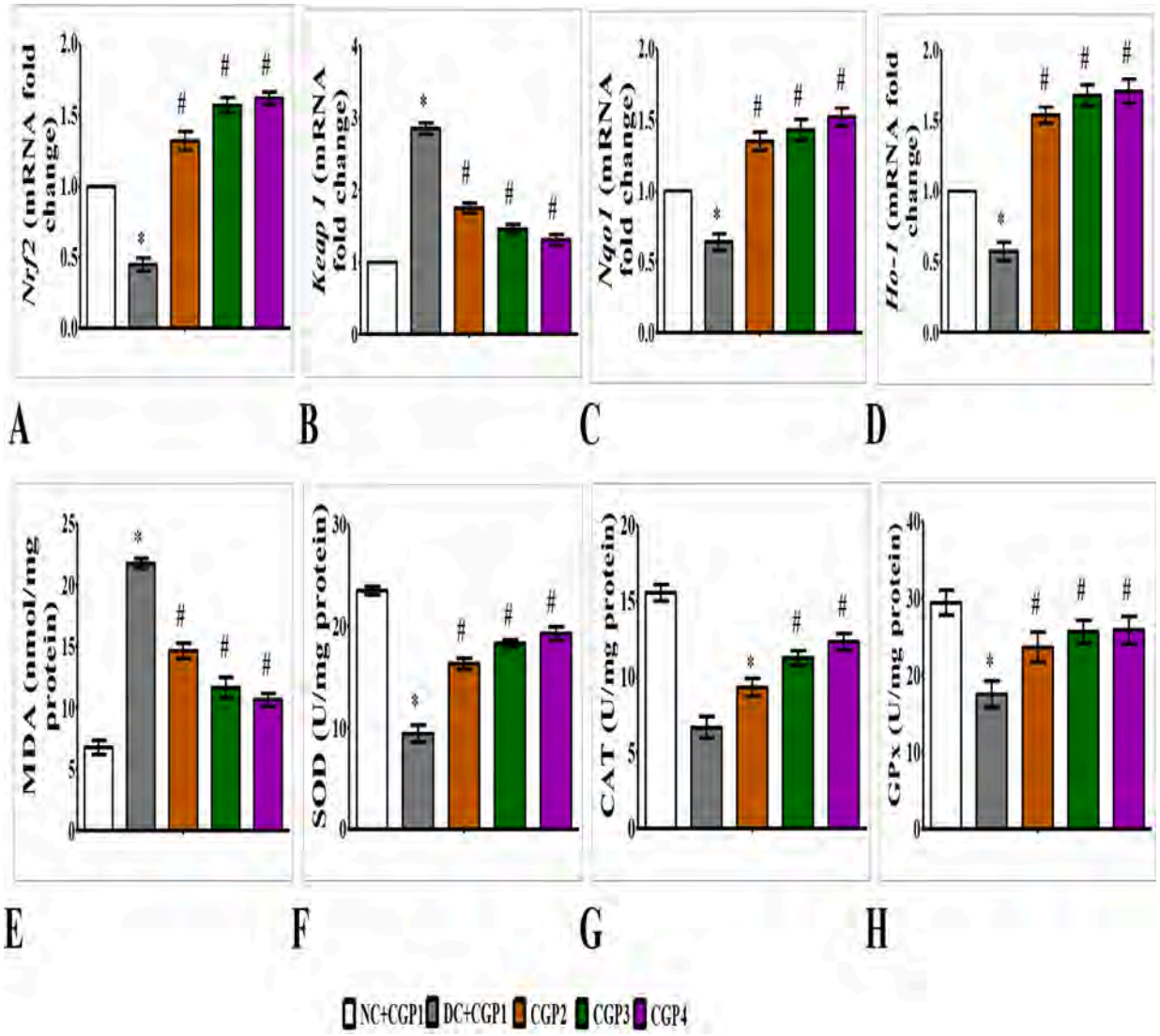


**Fig. 5.** Effect of GC-AgNP CGPs dressing on oxidative and anti-oxidative parameters in diabetic rats. Relative mRNA expression of **(A)** *Nrf2*; **(B)** *Keap 1*; **(C)** *Nqo1*; **(D)** *Ho-1*; **(E)** MDA; **(F)** SOD; **(G)** CAT; **(H)** GPx; NC + CGP1: Normal control dressed with blank cotton gauze; DC + CGP1: Diabetic control rats dressed with blank cotton gauze; CGP2: Diabetic rats dressed with 13.06 μM gallocatechin and silver nanoparticle (GC-AgNP) impregnated cotton gauze patches (DC+ 13.06 μM CGP2); CGP3: Diabetic rats dressed with 26.12 μM gallocatechin and silver nanoparticle (GC-AgNP) impregnated cotton gauze patches (DC+ 26.12 μM CGP3). CGP4: Diabetic rats dressed with silver sulfadiazine (DC + AgS) impregnated cotton gauze patches. Data were expressed as mean ± S.E.M ($n = 6$). *$p < 0.05$ compared to control, # $p < 0.05$ compared to DC.

### *3.15. Effect of GC-AgNP-CGPs on inflammation parameters in diabetic rats*

In order to determine the impact of GC-AgNP-CGP on inflammation in the wounds of diabetic rats, mRNA expression of inflammatory markers was assessed. The mRNA expressions of *Tlr4* (Fig. 7A), *Myd88* (Fig. 7B), *Nfkβ* (Fig. 7C), *Tnf-α* (Fig. 7E) and *Il-6* (Fig. 7F) were upregulated with downregulated mRNA expression of *Ikk-α* (Fig. 7D) in DC-CGP1 dressed rats healing skin when compared with DC-CGP1 dressed rats. However, *Tlr4*, *Myd88*, *Nfkβ*, *Tnf-α* and *Il-6* mRNA expression was downregulated with upregulated mRNA expression of *Ikb-α* in diabetic rats topical dressed with 13.06 μM CGP2 and 26.12 μM CGP3 when compared with DC-CGP1 dressed rats.

Supporting the observations of gene expression studies, immunohistochemistry and immunofluorescence studies revealed increased distribution of MYD88 (Fig. 7G), NFKβ p65 (Fig. 8A) and TNF-α (Fig. 8B) proteins was observed in DC-CGP1 dressed rats when compared to same distribution of proteins in NC-CGP1 dressed rats. In contrast, diabetic rats topical dressed with 13.06 μM CGP2 and 26.12 μM CGP3 showed lower distribution of MYD88, NFKβ p65 and TNF-α when compared to same protein distribution levels in DC-CGP1 dressed rats.

### *3.16. Effect of GC-AgNPs-CGPs on growth factors and MMP-2 in diabetic rats*

The distribution of growth factors such as VEGF (Fig. 9A), EGF (Fig. 9B), TGFβ (Fig. 9B) and FGF2 (Fig. 10A) decreased with increased distribution of MMP2 (Fig. 10B) in the DC-CGP1 dressed rats compared to NC-CGP1 dressed rats. In contrast, the distribution of VEGF, EGF, TGFβ and FGF2 was increased with decreased MMP2 in diabetic rats topical dressed with 13.06 μM CGP2 and 26.12 μM CGP3 compared to DC-CGP1 dressed rats.

## 4. Discussion

One of the most prominent clinical symptoms of diabetes is delayed wound healing. The cause of delayed wound healing in diabetes mellitus is multi-factorial, including elevated oxidative stress, chronic

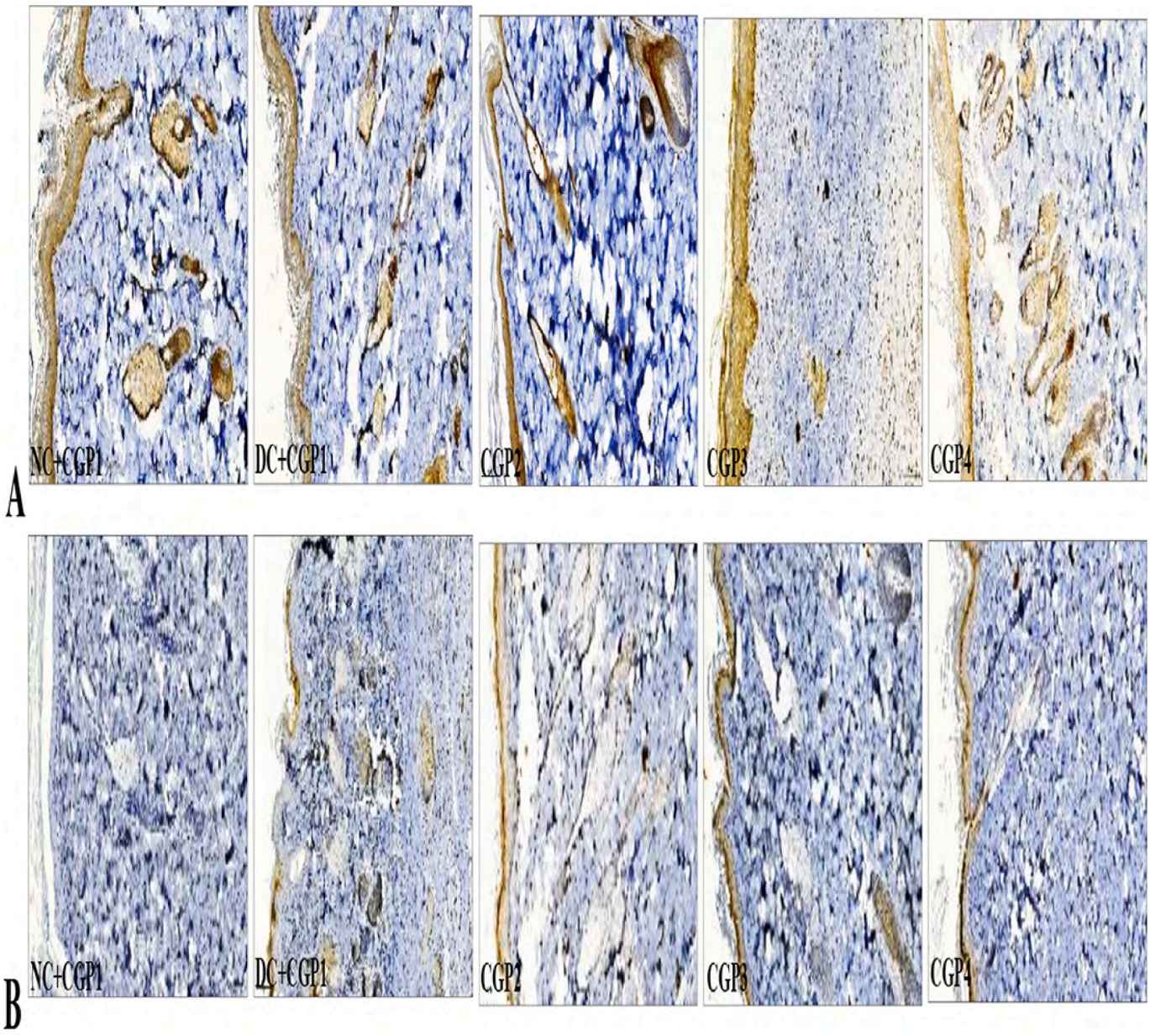


**Fig. 6.** Effect of GC-AgNP CGPs dressing on oxidative and anti-oxidative parameters in diabetic rats. Immunohistochemistry staining of **(A)** NRF2; **(B)** HO-1. NC + CGP1: Normal control dressed with blank cotton gauze; DC + CGP1: Diabetic control rats dressed with blank cotton gauze; CGP2: Diabetic rats dressed with 13.06 μM gallocatechin and silver nanoparticle (GC-AgNP) impregnated cotton gauze patches (DC+ 13.06 μM CGP2); CGP3: Diabetic rats dressed with 26.12 μM gallocatechin and silver nanoparticle (GC-AgNP) impregnated cotton gauze patches (DC+ 26.12 μM CGP3). CGP4: Diabetic rats dressed with silver sulfadiazine (DC + AgS) impregnated cotton gauze patches. Scale bar = 100 μm.

inflammation and changes in connective tissue and reduced collagen synthesis and reepithelialisation. Creation of animal models helps in studying the healing mechanism under diabetes milieu. In this study, streptozotocin (STZ) and nicotinamide were used for induction of diabetes in rats. STZ is a diabetic agent that damages pancreatic β cells, whereas nicotinamide partially prevented STZ induced pancreatic β cell damages, which subsequently resulted in a diabetic phenotype. A significant progress in diabetic wound healing using combinations of several metallic nanoparticles, polymers and polysaccharides have been reported in the literature. Silver ions due to their antimicrobial effects have been very effective and widely employed in wound dressings. Further, modifications to AgNPs have potentiated their antimicrobial profiles, surface modified silica and silver nanoparticles with 2-aminomethylpyridine (Si-TAMPy) and 8-hydroxyqinoloine (Si-TQ) exhibited a broad antibacterial profile [34]. In a study conducted by Abdelsalam et al. [35] on meristematic tissues of root tips detected chromosomal abnormalities in cells at >40 ppm concentrations of AgNPs. Conversely, both silver and gold nanoparticles demonstrated significant reduction in cardiotoxicity along with blackberry extract [36]. Fauda et al. [37] reported improved diabetic wound healing in rats by a glycoaminoglycan usually present in soft connective tissues commonly referred as hyaluronan. High concentrations of hyaluronan not only reduced the pathogenic microbes at the wound site but also reduced the markers associated with oxidative stress and toxicity. Similarly, accelerated wound healing was observed by El-Aassar et al. [38] when combination of hyaluronic acid, polygalactouronic acid and AgNPs were embedded in a nanofibrous wound dressing. Therefore, the current research is started by developing the GC-AgNPs impregnated cotton gauze patches and studying its role in wound healing. The GC-AgNPs-CGPs were well characterized for various physicochemical properties. The results

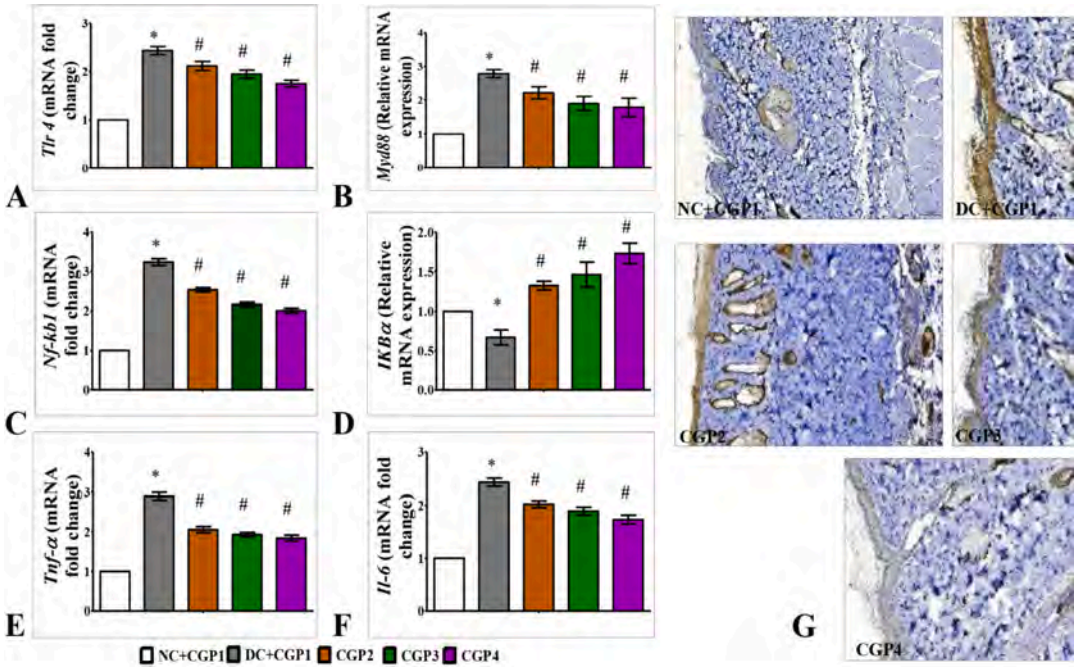


**Fig. 7.** Effect of GC-AgNP CGPs dressing on inflammation parameters in diabetic rats. Relative mRNA expression of **(A)** *Tlr4*; **(B)** *Myd88*; **(C)** *Nfkb*; **(D)** *Ikbα*; **(E)** *Tnf-α*; **(F)** *Il-6*; Immunohistochemistry staining of **(G)** MYD88; NC + CGP1: Normal control dressed with blank cotton gauze; DC + CGP1: Diabetic control rats dressed with blank cotton gauze; CGP2: Diabetic rats dressed with 13.06 μM gallocatechin and silver nanoparticle (GC-AgNP) impregnated cotton gauze patches (DC+ 13.06 μM CGP2); CGP3: Diabetic rats dressed with 26.12 μM gallocatechin and silver nanoparticle (GC-AgNP) impregnated cotton gauze patches (DC+ 26.12 μM CGP3). CGP4: Diabetic rats dressed with silver sulfadiazine (DC + AgS) impregnated cotton gauze patches. Data were expressed as mean ± S.E.M ($n = 6$). *$p < 0.05$ compared to control, # $p < 0.05$ compared to DC. Scale bar = 100 μm.

revealed that GC-AgNPs-CGPs accelerate wound healing in diabetic rats through its anti-diabetic, anti-oxidant and anti-inflammatory effects.

The appearance of prepared CGPs was homogenous with no air bubbles, brittleness, discolouration and fissures. Their physicochemical properties such as folding endurance, moisture content, GC/AgS content were acceptable and promote wound healing. The tensile strengths of GC-AgNP CGPs were evaluated as shown in Fig. 1. Initial linear section of the curve represents the elastic deformation of the patch. This is the stage where the patch is being stretched and this deformation can be reversed by removing the stress applied. The peak of the curve is known as tensile strength with the maximum stress value. Beyond this point, additional stress can cause permanent deformation and eventually progress to breaking point. From the results, CGP2 to CGP3 showed significant flexibility with good elasticity without break and can withstand stress during dressing application, dressing removal and during patient movement as seen in Fig. 1K.

To know the water absorption capabilities of GC-AgNPs-CGPs, water absorption test and vertical wicking tests were carried out. These CGPs had moderate water absorption, the water absorption of CGPs can be explained with diffusion mechanism proposed by Lukitowati and Indrani [39] where polar water molecules (ionised into $H^+$ and $OH^-$ ions) were trapped at the hydroxyl, ether and amine functional groups in chitosan film and hence causes weight gain when immersed in water. A wound dressing with good water absorption can absorb wound exudate and maintain moist healing environment. Moist wound treatment can promote tissue regeneration, accelerate wound healing, allow gentle dressing removal without interrupting freshly formed tissue and reduce scar formation [40–42].

The FTIR spectra of raw materials and CGPs are as shown in Fig. 2A. Chitosan is a biodegradable polymer of semi-crystalline properties. Its FTIR spectra showed functional peaks 1738.24 $cm^{-1}$ (N—H bending), 1366.79 $cm^{-1}$ (C—H stretching), 1216.28 $cm^{-1}$ (Phenol C—O band) and 1024.35 $cm^{-1}$ (N—C stretching). However, the intensity of O—H, C—O vibrations is not captured in the spectra. Their intensity has increased upon addition of AgNPs to the chitosan matrix of CGP spectra. In addition, a broad peak in the FTIR spectra of CGPs also suggests the solvent casting method used for the film formation. This is further confirmed by the absence of broad peak in the physical mixture of raw materials where solvent casting was not used. Pure GC showed functional peaks at 3203.57 $cm^{-1}$ (O—H stretching), 1691.79 $cm^{-1}$ (C═C stretching) and 1345.56 $cm^{-1}$ (Phenol C—O stretching) which are not prominent. Overall, CGPs did not exhibited any major functional group changes to indicate chemical interactions.

The DSC thermogram of pure chitosan polymer showed melting peak at 90.6 °C, in presence of AgNPs this shifted towards higher end. There was an increase in melting peaks of CGP2, CGP3 and CGP4 to 109.6, 114, 121.5 °C respectively. Besides the peak intensity was enhanced due to AgNPs presence. Presence of Gallocatechin, AgS enhanced the crystallinity of the CGPs noticed in the thermograms by reduced broadening of the peaks. The thermograms are dominated by the chitosan because its concentration is relatively higher than other components. Nevertheless, physical interactions were observed that altered the physical state causing shifts and changes in peak intensities.

The GC/AgS release and permeation in Franz diffusion cell revealed a sharp rise in receptor compartment concentration in the first 15 min of the study which dropped rapidly till 1 h. There could be a possibility that initial release is from the surface of CGPs and not from the matrix. Shrinkage of matrix layer may also be one of the reasons that might have caused initial burst release. It was assumed that considerable time is needed for GC/AgS to diffuse out from the inner part of the matrix giving a prolonged release character. This is correlated well with the vertical wicking test and static immersion test which revealed significantly lesser capillary action, water absorption by the other CGPs compared to CGP1. CGP2 revealed lesser permeation compared to CGP3, with higher concentration of GC in CGP3 higher concentration gradient is possible that can result in greater diffusion. It was also evident in higher flux observed in CGP3 than CGP2. Drug release rate is highly dependent on its diffusion from the pores of polymer matrix and diffusivity of the drug which

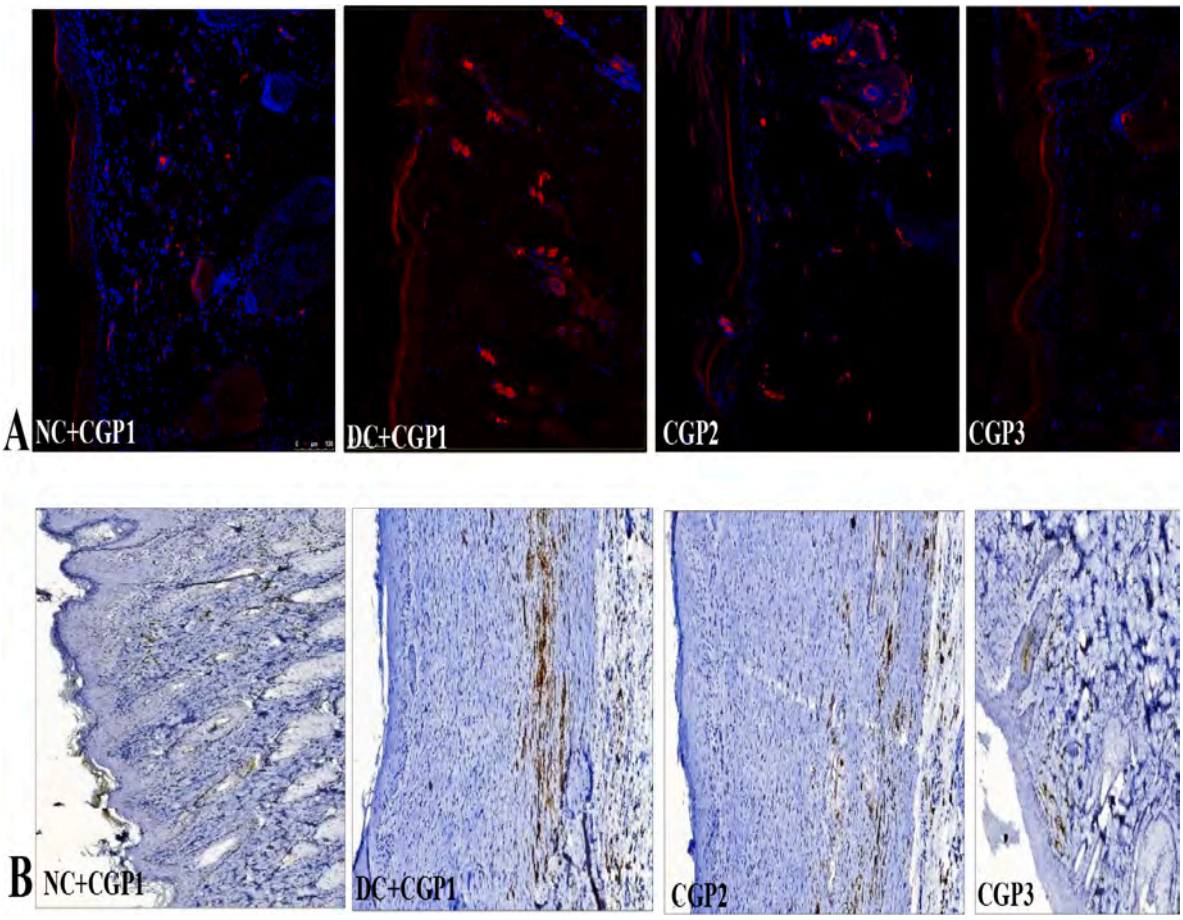


**Fig. 8.** Effect of GC-AgNP CGPs dressing on inflammation parameters in diabetic rats.
Immunofluorescence staining of **(A)** NFKβ p65 (Red colour); immunohistochemistry staining of **(B)** TNF-α. NC + CGP1: Normal control dressed with blank cotton gauze; DC + CGP1: Diabetic control rats dressed with blank cotton gauze; CGP2: Diabetic rats dressed with 13.06 μM gallocatechin and silver nanoparticle (GC-AgNP) impregnated cotton gauze patches (DC+ 13.06 μM CGP2); CGP3: Diabetic rats dressed with 26.12 μM gallocatechin and silver nanoparticle (GC-AgNP) impregnated cotton gauze patches (DC+ 26.12 μM CGP3). CGP4: Diabetic rats dressed with silver sulfadiazine (DC + AgS) impregnated cotton gauze patches. Data were expressed as mean ± S.E.M ($n = 6$). $^{*}p < 0.05$ compared to control, $\# p < 0.05$ compared to DC. Scale bar = 100 μm. (For interpretation of the references to colour in this figure legend, the reader is referred to the web version of this article.)

is indirectly proportional to its molecular weight [23]. Silver sulfadiazine might be chemically or electrostatically bound to the chitosan matrix resulting in incomplete release or sustained release.

Diabetic rats with blank cotton gauze patch showed significant decrease in body weight on days 6, 12 and 18 when compared to that of body weight in control rats with normal cotton gauze patch, while diabetic rats dressed with 13.06 μM CGP2 and 26.12 μM CGP3 prevented body weight loss that was observed in DC-CGP1 indicating improvement in body weight after treating diabetic wounds with 13.06 μM CGP2 and 26.12 μM CGP3. During the study, high levels of blood glucose were observed in DC-CGP1 rats when compared to NC-CGP1 rats. Conversely, 13.06 μM CGP2 and 26.12 μM CGP3 dressed diabetic rats showed fall in glucose levels when compared to DC-CGP1 rats demonstrating anti-glycemic effect of GC-AgNPs-CGPs. The results are well supported by Samarghandian et al. [9] who reported anti-hyperglycemic effect of catechin in the management of diabetes.

The gross wound size was higher with increased wound healing time in diabetic rats but decreased gross wound size with significant reduction in wound healing time was observed in 13.06 μM CGP2 and 26.12 μM CGP3 diabetic rats. These dressings facilitate healing in diabetic rats through antibacterial, anti-inflammatory, proangiogenic and proliferative properties. Earlier studies identified that topical application of (−)-epigallocatechin gallate improves wound healing in diabetic mice by enhancing wound contraction and reducing wound duration [43]. Histopathological studies supported the gross changes through increased re-epithelialization, neovascularisation, strong fibrous content with parallel structured collagen fibres, hair regrowth and a highly organized epidermal growth with keratinocytes in the skin after the application of 13.06 μM CGP2 and 26.12 μM CGP3 to diabetic rats. Besides, Masson trichrome stains confirm presence of increased presence of collagen on diabetic rat's skin dressed with 13.06 μM CGP2 and 26.12 μM CGP3. Previously, Negrão et al. [44] observed that catechins are capable of increasing the mechanism of angiogenesis, which is correlated with the present findings.

Experimental and clinical studies have shown that delay in diabetic wounds is associated with oxidative stress [3,45,46]. Even though reactive oxygen species (ROS) have been considered as critical regulators at different phases of wound healing, oxidative stress ensues when ROS outweigh the antioxidant defences that lead to delay in wound repair [47]. Earlier studies of Shaheen et al. [48] identified the role of gold and silver nanoparticles in successfully combating oxidative stress in diabetic rat model by elevating antioxidant defence and regulation of inflammatory markers IL-α and C-Reactive protein *via* reduced lipid profile. In this study, diabetic wound experienced high oxidizing environment in the form of elevated levels of MDA, a product of lipid peroxidation and reduced activities of antioxidant defences such as SOD, CAT and GPx. The present findings support earlier observations of elevated lipid peroxidation and compromised antioxidant defences [3].

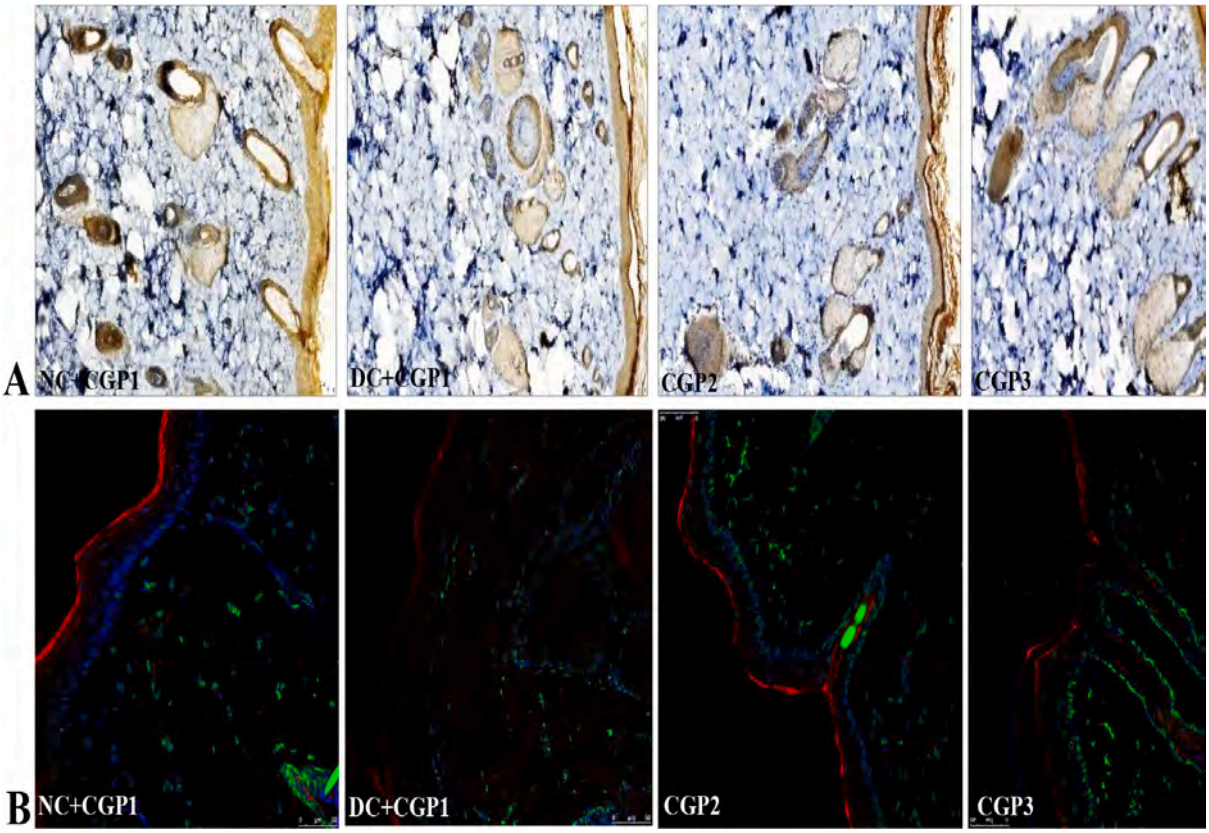


**Fig. 9.** Effect of GC-AgNP CGPs dressing on growth factors in diabetic rats. Immunohistochemistry staining of **(A)** VEGF; Immunofluorescence double staining images showing co-localization of **(B)** EGF (red) and TGFβ (green). NC + CGP1: Normal control dressed with blank cotton gauze; DC + CGP1: Diabetic control rats dressed with blank cotton gauze; CGP2: Diabetic rats dressed with 13.06 μM gallocatechin and silver nanoparticle (GC-AgNP) impregnated cotton gauze patches (DC+ 13.06 μM CGP2); CGP3: Diabetic rats dressed with 26.12 μM gallocatechin and silver nanoparticle (GC-AgNP) impregnated cotton gauze patches (DC+ 26.12 μM CGP3). CGP4: Diabetic rats dressed with silver sulfadiazine (DC + AgS) impregnated cotton gauze patches. Data were expressed as mean ± S.E.M (n = 6). Scale bar = 100 μm. (For interpretation of the references to colour in this figure legend, the reader is referred to the web version of this article.)

Conversely, diabetic rats dressed with 13.06 μM CGP2 and 26.12 μM CGP3 showed increased levels of MDA with reduced enzymes activities of SOD, CAT and GPx in the healing tissue is an indication of reduced oxidative stress in wound area. Previously, Oršolić et al. [49] found that epigallocatechin gallate reduces oxidative stress levels in diabetic mice.

To know the in-depth mechanisms behind de-regulation of oxidative status, Nrf2 pathway is studied as previous studies pointed out that Nrf2 suppression delays wound healing through consistent oxidative stress and inflammation [50]. *In vitro* and *in vivo* experiments showed that suppression of Nrf2 activation hampers wound repair and activation of Nrf2 accelerates wound repair by attenuating oxidative stress and inflammation [50]. DC-CGP1 dressed rat healing tissues exhibited lower mRNA expression of *Nrf2, Nqo1* and *Ho-1* and protein distribution of *Nrf2* with higher mRNA expression and protein distribution of *Keap-1* when compared to respective mRNA and protein distribution in NC-CGP1 dressed rats. However, there was upregulated mRNA expression of *Nrf2*, *Nqo1* and *Ho-1*) and increased protein distribution of *Nrf2* with reduced mRNA expression and protein distribution of *Keap-1* in 13.06 μM CGP2 and 26.12 μM CGP3 dressed diabetic rats demonstrating the involvement of activated Nrf2 and its associated factors in the modulation of oxidative stress.

Although low level inflammation including generation of pro-inflammatory mediators is a common feature and beneficial to heal wounds [51], some external stimulus including hyperglycemia makes wounds stuck in a persistent inflammatory state [3,50,52] that halts the wound healing process. In addition, there are studies which reported the involvement of oxidative stress in the aggravation of inflammatory condition [50]. Earlier it was reported that activation of NF-κB is involved in development and progression of inflammation [53]. Normally in the cytoplasm NF-kB stays inactive in association with IκBα and upon activation IκBα gets degraded and then NF-kB translocates to nucleus to activate effectors of inflammation [54]. Of note, the involvement of TLR4 and MYD88 in the activation of NF-kB and thereby elevated expression of inflammatory effectors is also evidenced [54]. In this study, DC-CGP1 dressed rats presented with elevated mRNA expression of *Tlr4*, *Myd88*, *Nfkβ*, *Tnf-α* and *Il-6* and protein distribution of MYD88, NF-kB p65 and TNF-α with reduced mRNA expression of *Ikb-α*. It indicates the activation of TLR4/MYD88/NF-kB pathway and stimulation of inflammatory effectors (*Tnf-α* and *Il-6*) thereby stops healing of diabetic wound. In contrast, dressing of diabetic wounds with 13.06 μM CGP2 and 26.12 μM CGP3 significantly improved wound healing through inactivation of TLR4/MYD88/NF-kB pathway and suppression of effectors of inflammation.

Plethora of scientific reports claimed the importance of growth factors such as VEGF, EGF, TGFβ and FGF in neovascularisation or angiogenesis and role of collagen synthesis in the promotion of wound healing through granular tissue formation [55–60]. Collagen synthesis has been considered as most critical event in wound healing as its organization into thick bundles makes tissue strong. Previous studies also reported the involvement of MMPs in delaying of wound healing through its degrading ability on extracellular matrix [61,62]. In the present study, diabetic wound caused reduced protein distribution of VEGF, EGF, TGFβ and FGF with elevated distribution of MMP2 protein and reduced collagen synthesis. Conversely, distribution of VEGF, EGF, TGFβ and FGF2 was elevated with reduced distribution of MMP2 and increased collagen synthesis in diabetic rats topical dressed with 13.06 μM CGP2

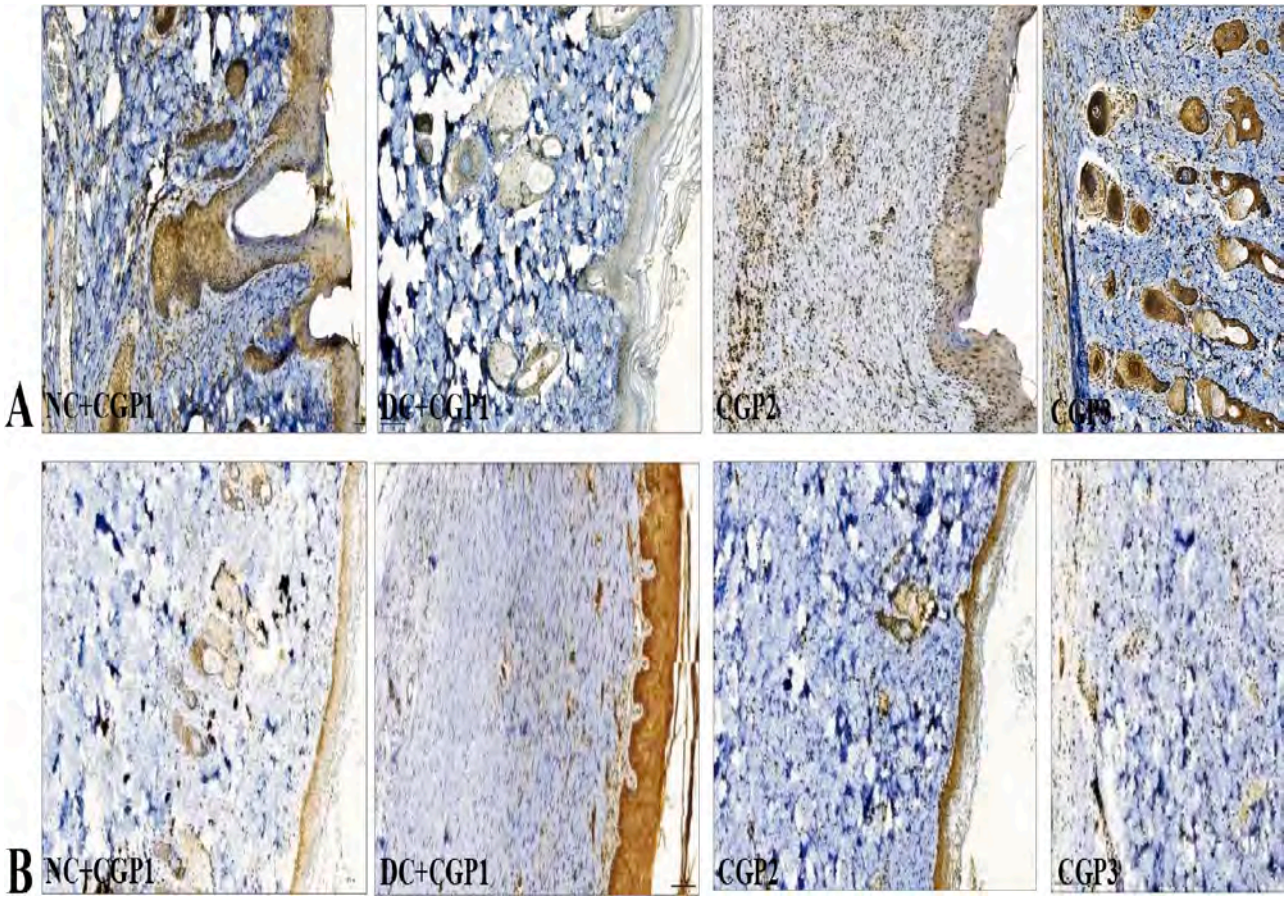


**Fig. 10.** Effect of GC-AgNP CGPs dressing on growth factors and MMP-2 in diabetic rats. Immunohistochemistry staining of **(A)** FGF2; **(B)** MMP2. NC + CGP1: Normal control dressed with blank cotton gauze; DC + CGP1: Diabetic control rats dressed with blank cotton gauze; CGP2: Diabetic rats dressed with 13.06 μM gallocatechin and silver nanoparticle (GC-AgNP) impregnated cotton gauze patches (DC+ 13.06 μM CGP2); CGP3: Diabetic rats dressed with 26.12 μM gallocatechin and silver nanoparticle (GC-AgNP) impregnated cotton gauze patches (DC+ 26.12 μM CGP3). CGP4: Diabetic rats dressed with silver sulfadiazine (DC + AgS) impregnated cotton gauze patches. Data were expressed as mean ± S.E.M (n = 6). Scale bar = 100 μm.

and 26.12 μM CGP3 when compared to DC-CGP1 dressed rats indicating activation of growth factors, suppression of MMP-2 and increased collagen synthesis thereby helped in faster healing of diabetic wound.

The biochemical and molecular analyses data are well supported by histopathological observations in the study. CGP1 dressed diabetic rats showed serious histologic alterations in the form of loss of epithelial cover, inflammatory cell infiltrations and empty spaces. While, diabetic rats dressed with 13.06 μM CGP2 and 26.12 μM CGP3 showed significant improvement in the form of optimal re-epithelisation, epidermal remodelling, dermal reconstruction and the surface was fully covered by a thick sero-cellular crust composed of necrotic tissue debris and inflammatory exudates with increased collagen content.

In conclusion, the prepared CGP2, CGP3 and CGP4 formulations were characterized for various physicochemical properties. The CGPs demonstrated insignificant weight variation, thickness, but possesses good tensile strength, folding endurance prerequisite for transdermal applications. Besides, low moisture levels to check microbial growth and higher water absorption capabilities are ideal for exuding wounds. The *in vitro* permeation study on CGP2 and CGP3 revealed that GC can permeate rapidly with a flux of 0.061 and 0.143 mg/sq.cm/h and more than 83.21% in 2 h. Further, *in vivo* wound healing ability in animal model is significantly improved by 13.06 μM CGP2 and 26.12 μM CGP3. The improvement might be due to its antioxidant, anti-inflammatory properties with increased growth factors and reduced matrix metalloproteinase. Altogether, 13.06 μM CGP2 and 26.12 μM CGP3 due to immediate release of GC showed significant improvement in wound healing and it could be a potential therapy to treat diabetic wounds, further clinical studies are warranted before its clinical use.

## Funding

This research was funded by Geran Penyelidikan Universiti Malaya (UMRG) grant, Universiti Malaya, Malaysia (Project no. RG372-15AFR).

## Declaration of competing interest

All the authors read and agreed the manuscript to be submitted and there is no conflict among the author and other parties.

## References

[1] K. Ogurtsova, J.D. da Rocha Fernandes, Y. Huang, U. Linnenkamp, L. Guariguata, N.H. Cho, D. Cavan, J.E. Shaw, L.E. Makaroff, IDF Diabetes Atlas: Global estimates for the prevalence of diabetes for 2015 and 2040, Diabetes Res. Clin. Pract. 128 (2017) 40–50.
[2] S. Patel, S.D. Dwivedi, K. Yadav, J.R. Kanwar, M.R. Singh, D. Singh, Pathogenesis and molecular targets in treatment of diabetic wounds, in: Obesity and Diabetes, Springer, Cham, 2020, pp. 747–758.
[3] J. Ren, M. Yang, F. Xu, J. Chen, S. Ma, Acceleration of wound healing activity with syringic acid in streptozotocin induced diabetic rats, Life Sci. 233 (2019), 116728.
[4] I. Bellezza, I. Giambanco, A. Minelli, R. Donato, Nrf2-Keap1 signaling in oxidative and reductive stress 1865 (5) (2018) 721–733.
[5] A. Jindam, V.G. Yerra, A. Kumar, Nrf2: A promising trove for diabetic wound healing, Ann. Trans. Med. 5 (23) (2017).
[6] J.Y. Park, J. Lee, M. Jeong, S. Min, S.Y. Kim, H. Lee, Y. Lim, H.J. Park, Effect of Hominis placenta on cutaneous wound healing in normal and diabetic mice, Aug, Nutr. Res. Pract. 8 (4) (2014) 404–409.

[7] J.J. Salazar, W.J. Ennis, T.J. Koh, Diabetes medications: impact on inflammation and wound healing, J. Diabetes Complicat. 30 (4) (2016) 746–752.
[8] E. Karthikeyan, M.R.V. Pawar, ROLE OF CATECHINS IN DIABETES MELLITUS, European Journal of Molecular & Clinical Medicine 8 (2) (2021) 1730–1735.
[9] S. Samarghandian, M. Azimi-Nezhad, T. Farkhondeh, Catechin treatment ameliorates diabetes and its complications in streptozotocin-induced diabetic rats, Dose-Response 15 (1) (2017).
[10] G.W. Plumb, S. de Pascual-Teresa, C. Santos-Buelga, J.C. Rivas-Gonzalo, G. Williamson, Antioxidant properties of gallocatechin and prodelphinidins from pomegranate peel, Redox. Rep. 7 (1) (2002) 41–46.
[11] M. Ashtikar, M.G. Wacker, Nanopharmaceuticals for wound healing–lost in translation? Adv. Drug Deliv. Rev. 129 (2018) 194–218.
[12] N.K. Rajendran, S.S.D. Kumar, N.N. Houreld, H. Abrahamse, A review on nanoparticle based treatment for wound healing, J.Drug Deliv. Sci. Technol. 44 (2018) 421–430.
[13] M.G. Mehrabani, R. Karimian, B. Mehramouz, M. Rahimi, H.S. Kafil, Preparation of biocompatible and biodegradable silk fibroin/chitin/silver nanoparticles 3D scaffolds as a bandage for antimicrobial wound dressing, Int. J. Biol. Macromol. 114 (2018) 961–971.
[14] D. Simões, S.P. Miguel, M.P. Ribeiro, P. Coutinho, A.G. Mendonça, I.J. Correia, Recent advances on antimicrobial wound dressing: a review, Eur. J. Pharm. Biopharm. 127 (2018) 130–141.
[15] V.S. Radhakrishnan, M.K.R. Mudiam, M. Kumar, S.P. Dwivedi, S.P. Singh, T. Prasad, Silver nanoparticles induced alterations in multiple cellular targets, which are critical for drug susceptibilities and pathogenicity in fungal pathogen (Candida albicans), Int. J. Nanomedicine 13 (2018) 2647.
[16] W.M. Dosoky, M. Fouda, A.B. Alwan, N.R. Abdelsalam, A.E. Taha, R.Y. Ghareeb, M. R. El-Aassar, A.F. Khafaga, Dietary supplementation of silver-silica nanoparticles promotes histological, immunological, ultrastructural, and performance parameters of broiler chickens, Sci. Rep. 11 (1) (2021) 4166.
[17] M. Fouda, W.M. Dosoky, N.S. Radwan, N.R. Abdelsalam, A.E. Taha, A.F. Khafaga, Oral administration of silver nanoparticles-adorned starch as a growth promotor in poultry: Immunological and histopathological study, Int. J. Biol. Macromol. 187 (2021) 830–839.
[18] M. Fouda, N.R. Abdelsalam, I. Gohar, A. Hanfy, S.I. Othman, A.F. Zaitoun, A. A. Allam, O.M. Morsy, M. El-Naggar, Utilization of high throughput microcrystalline cellulose decorated silver nanoparticles as an eco-nematicide on root-knot nematodes, Colloids Surf. B: Biointerfaces 188 (2020), 110805.
[19] M. Fouda, N.R. Abdelsalam, M.E. El-Naggar, A.F. Zaitoun, B. Salim, M. Bin-Jumah, A.A. Allam, S.A. Abo-Marzoka, E.E. Kandil, Impact of high throughput green synthesized silver nanoparticles on agronomic traits of onion, Int. J. Biol. Macromol. 149 (2020) 1304–1317.
[20] A. Moeini, P. Pedram, P. Makvandi, M. Malinconico, G.G. d'Ayala, Wound healing and antimicrobial effect of active secondary metabolites in chitosan-based wound dressings: a review, Carbohydr. Polym. 233 (2020), 115839.
[21] M.R. El-Aassar, O.M. Ibrahim, M. Fouda, H. Fakhry, J. Ajarem, S.N. Maodaa, A. A. Allam, E.E. Hafez, Wound dressing of chitosan-based-crosslinked gelatin/polyvinyl pyrrolidone embedded silver nanoparticles, for targeting multidrug resistance microbes, Carbohydr. Polym. 255 (2021), 117484.
[22] D. Nirmala, S. Nandhini, M. Sudhakar, Design and evaluation of fast dissolving oral films of Zolpidem by solvent casting method, Asian J. Pharm. Res. 6 (2) (2016) 67–71.
[23] G.D. Venkatasubbu, T. Anusuya, Investigation on curcumin nanocomposite for wound dressing, Int. J. Biol. Macromol. 98 (2017) 366–378.
[24] H. Ohkawa, N. Ohishi, K. Yagi, Assay for lipid peroxides in animal tissues by thiobarbituric acid reaction, Jun, Anal. Biochem. 95 (2) (1979) 351–358.
[25] H.P. Misra, I. Fridovich, The role of superoxide anion in the autoxidation of epinephrine and a simple assay for superoxide dismutase, J. Biol. Chem. 247 (10) (1972) 3170–3175. May 25.
[26] A.C. Maehly, B. Chance, The assay of catalases and peroxidases, Methods Biochem. Anal. 1 (1954) 357–424.
[27] J.T. Rotruck, A.L. Pope, H.E. Ganther, A.B. Swanson, D.G. Hafeman, W. G. Hoekstra, Selenium: biochemical role as a component of glutathione peroxidase, Science 179 (4073) (1973) 588–590. Feb 9.
[28] H. Ali, R. Saad, A. Ahmed, B. El-Haj, A study of light influence on silver sulfadiazine cream: causes, effects, and solutions, Int. J. Pharm. Pharm. Res. 5 (2) (2016) 139–152.
[29] J.S. Boateng, K.H. Matthews, H.N. Stevens, G.M. Eccleston, Wound healing dressings and drug delivery systems: a review, J. Pharm. Sci. 97 (8) (2008) 2892–2923.
[30] J. Boateng, R. Burgos-Amador, O. Okeke, H. Pawar, Composite alginate and gelatin based bio-polymeric wafers containing silver sulfadiazine for wound healing, Int. J. Biol. Macromol. 79 (2015) 63–71.
[31] P.S. Das, P. Saha, Design and characterisation of transdermal patches of phenformin hydrochloride, Int. J. Curr. Pharm. Res. 9 (6) (2017) 90–93.
[32] T. Maver, S. Hribernik, T. Mohan, D.M. Smrke, U. Maver, K. Stana-Kleinschek, Functional wound dressing materials with highly tunable drug release properties, RSC Adv. 5 (2015) 77873–77884.
[33] L. Vinklárková, R. Masteikova, G. Foltýnová, J. Muselik, S. Pavloková, J. Bernatonienė, D. Vetchý, Film wound dressing with local anesthetic based on insoluble carboxymethycellulose matrix, J. Appl. Biomed. 15 (4) (2017) 313–320.
[34] K.A. Dahlous, O.H. Abd Elkader, M.G. Fouda, Z. Alothman, A. El-Faham, Eco-friendly method for silver nanoparticles immobilized decorated silica: Synthesis & characterization and preliminary antibacterial activity, J. Taiwan Inst. Chem. Eng. 95 (2019) 324–331.
[35] N.R. Abdelsalam, M. Fouda, A. Abdel-Megeed, J. Ajarem, A.A. Allam, M.E. El-Naggar, Assessment of silver nanoparticles decorated starch and commercial zinc nanoparticles with respect to their genotoxicity on onion, Int. J. Biol. Macromol. 133 (2019) 1008–1018.
[36] J. Hussein, M.E. El-Naggar, M. Fouda, O.M. Morsy, J.S. Ajarem, A.M. Almalki, A. A. Allam, E.M. Mekawi, The efficiency of blackberry loaded AgNPs, AuNPs and Ag@AuNPs mediated pectin in the treatment of cisplatin-induced cardiotoxicity in experimental rats, Int. J. Biol. Macromol. 159 (2020) 1084–1093.
[37] M.M. Fouda, A.M. Abdel-Mohsen, H. Ebaid, I. Hassan, J. Al-Tamimi, R.M. Abdel-Rahman, A. Metwalli, I. Alhazza, A. Rady, A. El-Faham, J. Jancar, Wound healing of different molecular weight of hyaluronan; in-vivo study, Int. J. Biol. Macromol. 89 (2016) 582–591.
[38] M.R. El-Aassar, O.M. Ibrahim, M. Fouda, N.G. El-Beheri, M.M. Agwa, Wound healing of nanofiber comprising polygalacturonic/hyaluronic acid embedded silver nanoparticles: in-vitro and in-vivo studies, Carbohydr. Polym. 238 (2020), 116175.
[39] F. Lukitowati, D.J. Indrani, Water Absorption of Chitosan, Collagen, and Chitosan/Collagen Blend Membranes Exposed to Gamma-Ray Irradiation, Iran. J. Pharm. Sci. 14 (1) (2018) 57–66.
[40] J. Cao, J. Wang, C.P. Jackman, A.H. Cox, M.A. Trembley, J.J. Balowski, B.D. Cox, D.E.A. Simone, A.L. Dickson, D.I.S. Talia, et al., Tension creates an endoreplication wavefront that leads regeneration of epicardial tissue, Dev. Cell 42 (2017) 600–615.e4.
[41] J.P. Junker, R.A. Kamel, E.J. Caterson, E. Eriksson, Clinical impact upon wound healing and inflammation in moist, wet, and dry environments, Sep, Adv. Wound Care (New Rochelle). 2 (7) (2013) 348–356.
[42] L. Liang, R.C. Stone, O. Stojadinovic, H. Ramirez, I. Pastar, A.G. Maione, A. Smith, V. Yanez, A. Veves, R.S. Kirsner, J.A. Garlick, M. Tomic-Canic, Integrative analysis of miRNA and mRNA paired expression profiling of primary fibroblast derived from diabetic foot ulcers reveals multiple impaired cellular functions, Nov, Wound Repair Regen. 24 (6) (2016) 943–953.
[43] Y.W. Huang, Q.Q. Zhu, X.Y. Yang, H.H. Xu, B. Sun, X.J. Wang, J. Sheng, Wound healing can be improved by (—)-epigallocatechin gallate through targeting Notch in streptozotocin-induced diabetic mice, FASEB J. 33 (1) (2019) 953–964.
[44] R. Negrão, R. Costa, D. Duarte, T.T. Gomes, I. Azevedo, R. Soares, Different effects of catechin on angiogenesis and inflammation depending on VEGF levels, Feb, J. Nutr. Biochem. 24 (2) (2013) 435–444.
[45] L. Deng, C. Du, P. Song, T. Chen, S. Rui, D.G. Armstrong, W. Deng, Therole of oxidative stress and antioxidants in diabetic wound healing, 2021.
[46] J. Dworzanski, M. Strycharz-Dudziak, E. Kliszczewska, M. Kiełczykowska, A. Dworzańska, B. Drop, M. Polz-Dacewicz, Glutathione peroxidase (GPx) and superoxide dismutase (SOD) activity in patients with diabetes mellitus type 2 infected with Epstein-Barr virus, Plos one 15 (3) (2020), e0230374.
[47] C. Dunnill, T. Patton, J. Brennan, J. Barrett, M. Dryden, J. Cooke, D. Leaper, N. T. Georgopoulos, Reactive oxygen species (ROS) and wound healing: the functional role of ROS and emerging ROS-modulating technologies for augmentation of the healing process, Int. Wound J. 14 (1) (2017) 89–96.
[48] T.I. Shaheen, M.E. El-Naggar, J.S. Hussein, M. El-Bana, E. Emara, Z. El-Khayat, M. Fouda, H. Ebaid, A. Hebeish, Antidiabetic assessment; in vivo study of gold and core-shell silver-gold nanoparticles on streptozotocin-induced diabetic rats 83 (2016) 865–875.
[49] N. Oršolić, D. Sirovina, G. Gajski, V. Garaj-Vrhovac, M.J. Jembrek, I. Kosalec, Assessment of DNA damage and lipid peroxidation in diabetic mice: effects of propolis and epigallocatechin gallate (EGCG) 757 (1) (2013) 36–44.
[50] M. Li, H. Yu, H. Pan, X. Zhou, Q. Ruan, D. Kong, Z. Chu, H. Li, J. Huang, X. Huang, A. Chau, Nrf2 suppression delays diabetic wound healing through sustained oxidative stress and inflammation, Front. Pharmacol. 10 (2019) 1099.
[51] R. Zhao, H. Liang, E. Clarke, C. Jackson, M. Xue, Inflammation in chronic wounds, Int. J. Mol. Sci. 17 (12) (2016) 2085.
[52] K.M. Cunnion, N.K. Krishna, H.K. Pallera, A. Pineros-Fernandez, M.G. Rivera, P. S. Hair, B.P. Lassiter, R. Huyck, M.A. Clements, A.F. Hood, G.T. Rodeheaver, Complement activation and STAT4 expression are associated with early inflammation in diabetic wounds, PLoS One 12 (1) (2017), e0170500.
[53] T. Liu, L. Zhang, D. Joo, S.C. Sun, NF-κB signaling in inflammation, Signal Transduct. Target Ther. 2 (2017) 17023, https://doi.org/10.1038/sigtrans.2017.23.
[54] S.V. Suryavanshi, Y.A. Kulkarni, NF-κβ: a potential target in the management of vascular complications of diabetes, Nov, Front. Pharmacol. 7 (8) (2017) 798.
[55] P. Bao, A. Kodra, M. Tomic-Canic, et al., The role of vascular endothelial growth factor in wound healing, J. Surg. Res. 153 (2) (2009) 347–358.
[56] S. Barrientos, H. Brem, O. Stojadinovic, et al., Clinical application of growth factors and cytokines in wound healing, Wound Repair Regen. 22 (5) (2014) 569–578.
[57] T.N. Demidova-Rice, M.R. Hamblin, I.M. Herman, Acute and impaired wound healing: pathophysiology and current methods for drug delivery, Part 2: role of growth factors in normal and pathological wound healing: therapeutic potential and methods of delivery, Adv. Skin Wound Care 25 (8) (2012) 349–370.
[58] K.E. Johnson, T.A. Wilgus, Vascular endothelial growth factor and angiogenesis in the regulation of cutaneous wound repair, Adv. Wound Care. 3 (10) (2014) 647–661.
[59] M.K. Lichtman, M. Otero-Vinas, V. Falanga, Transforming growth factor beta (TGF-beta) isoforms in wound healing and fibrosis, Wound Rep. Reg. 24 (2) (2016) 215–222.

[60] M. Pakyari, A. Farrokhi, M.K. Maharlooei, et al., Critical role of transforming growth factor beta in different phases of wound healing, Adv. Wound Care 2 (5) (2013) 215–224.

[61] S.M. Ayuk, H. Abrahamse, N.N. Houreld, The role of matrix metalloproteinases in diabetic wound healing in relation to photobiomodulation, J. Diabetes Res. 2016 (2016) 1–9.

[62] M. Xue, C.J. Jackson, Extracellular matrix reorganization during wound healing and its impact on abnormal scarring, Adv. Wound Care. 4 (3) (2015) 119–136.